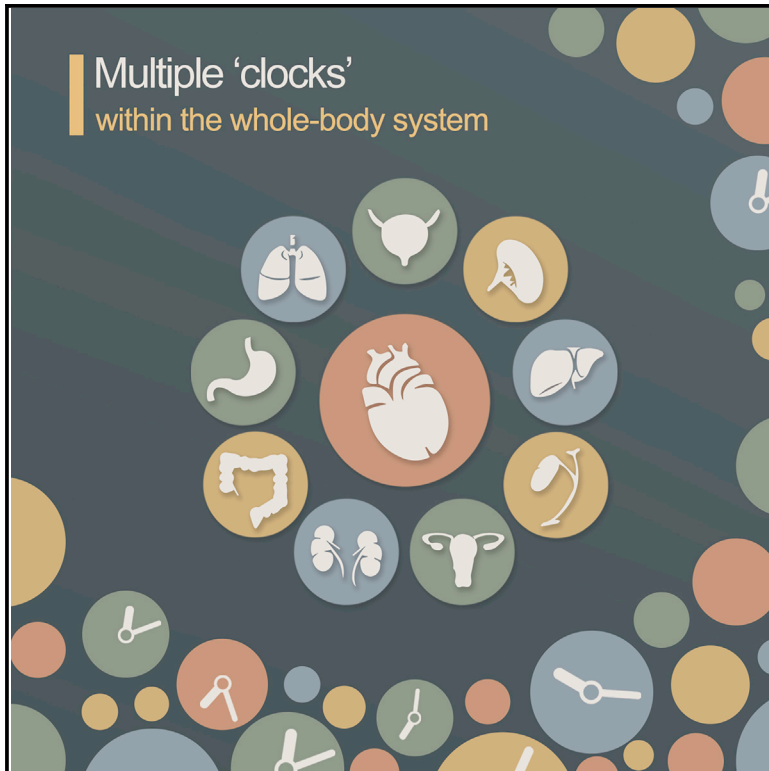


Distinct biological ages of organs and systems identified from a multi-omics study

Graphical abstract



Authors

Chao Nie, Yan Li, Rui Li, ..., Claudio Franceschi, Brian K. Kennedy, Xun Xu

Correspondence

xuxun@genomics.cn (X.X.), bkennedy@nus.edu.sg (B.K.K.), claudio.franceschi@unibo.it (C.F.), zhangxq@genomics.cn (X.Z.)

In brief

Nie et al. estimate biological ages of organs and systems using 402 multi-omics features from 4,066 individuals and demonstrate several applications. They find that organs and systems are aging at different rates, and biological ages could be utilized for population stratification, mortality prediction, and phenotypes of genetic association studies.

Highlights

- Constructing biological ages of organs/systems using multi-omics features
- Organs and systems are aging at different rates
- Specific biological age could predict disease of corresponding organs
- Biological ages of organs and systems have diverse genetic architectures



Article

Distinct biological ages of organs and systems identified from a multi-omics study

Chao Nie,^{1,2,10} Yan Li,^{1,2,10} Rui Li,^{1,2,10} Yizhen Yan,^{1,2} Detao Zhang,^{1,2} Tao Li,^{1,2} Zhiming Li,^{1,2} Yuzhe Sun,^{1,2} Hefu Zhen,^{1,2} Jiahong Ding,^{1,2} Ziyun Wan,^{1,2} Jianping Gong,³ Yanfang Shi,⁴ Zhibo Huang,^{1,2} Yiran Wu,^{1,2} Kaiye Cai,^{1,2} Yang Zong,¹ Zhen Wang,¹ Rong Wang,¹ Min Jian,^{1,2} Xin Jin,^{1,2} Jian Wang,^{1,2} Huanming Yang,^{1,2} Jing-Dong J. Han,⁵ Xiuqing Zhang,^{1,2,*} Claudio Franceschi,^{6,*} Brian K. Kennedy,^{7,8,9,*} and Xun Xu^{1,2,11,*}

¹BGI-Shenzhen, Shenzhen 518083, China

²China National GeneBank, Shenzhen 518120, China

³Medical Examination Center, The Affiliated Hospital of Hebei University, Baoding 071000, China

⁴Department of Neurosurgery, The Affiliated Hospital of Hebei University, Baoding 071000, China

⁵Peking-Tsinghua Center for Life Sciences, Academy for Advanced Interdisciplinary Studies, Center for Quantitative Biology (CQB), Peking University, Beijing 100871, China

⁶Institute of Information Technologies, Mathematics and Mechanics, Lobachevsky State University, Nizhny Novgorod, Russia

⁷Healthy Longevity Translation Research Programme, Yong Loo Lin School of Medicine, National University of Singapore, Singapore, Singapore

⁸Centre for Health Longevity, National University Health System, Singapore, Singapore

⁹Singapore Institute of Clinical Sciences, Agency for Science, Technology and Research (A*STAR), Singapore, Singapore

¹⁰These authors contributed equally

¹¹Lead contact

*Correspondence: xuxun@genomics.cn (X.X.), bkennedy@nus.edu.sg (B.K.K.), claudio.franceschi@unibo.it (C.F.), zhangxq@genomics.cn (X.Z.)
<https://doi.org/10.1016/j.celrep.2022.110459>

SUMMARY

Biological age (BA) has been proposed to evaluate the aging status instead of chronological age (CA). Our study shows evidence that there might be multiple “clocks” within the whole-body system: systemic aging drivers/clocks overlaid with organ/tissue-specific counterparts. We utilize multi-omics data, including clinical tests, immune repertoire, targeted metabolomic molecules, gut microbiomes, physical fitness examinations, and facial skin examinations, to estimate the BA of different organs (e.g., liver, kidney) and systems (immune and metabolic system). The aging rates of organs/systems are diverse. People’s aging patterns are different. We also demonstrate several applications of organs/systems BA in two independent datasets. Mortality predictions are compared among organs’ BA in the dataset of the United States National Health and Nutrition Examination Survey. Polygenic risk score of BAs constructed in the Chinese Longitudinal Healthy Longevity Survey cohort can predict the possibility of becoming centenarian.

INTRODUCTION

The aging process is the major risk factor for disease and death (Harman, 1991). The aging rate varies for different people at the same chronological age (CA); thus, biological age (BA) was developed to assess the true aging rate (Franceschi et al., 2018). The concept of BA has been investigated since the 1970s (Comfort, 1969). Multiple methods were developed later, including multiple linear regression (Bae et al., 2008; Cho et al., 2010; Dubina et al., 1984; Hollingsworth et al., 1965; Krøll and Saxtrup, 2000), principal component analysis (Hofecker et al., 1980; Nakamura and Miyao, 2007; Nakamura et al., 1988), and the Klemmera and Doubal method (KMD) (Klemmera and Doubal, 2006). The major difference among these methods is the role of CA. In the earlier multiple linear regression studies (Bae et al., 2008; Krøll and Saxtrup, 2000), CA was predicted from biomarkers. It was believed that the higher the correlation between

biomarker and CA, the greater the reliability of BA estimation. The later algorithm used reverse regression and treated CA also as a marker of aging (Klemmera and Doubal, 2006). Both strategies have been applied in multiple datasets, where KMD was shown to have better performances in mortality (Levine, 2013) and health status predictions (Cho et al., 2010).

Another key factor for estimating BA is selection of age-related biomarkers. Over the last half century, electronic medical records, DNA methylation (Horvath et al., 2015; Horvath and Raj, 2018), transcriptome (Stegeman and Weake, 2017), and proteome signatures (Lehallier et al., 2019) have been used for estimating BA, whereby DNA methylation has been shown to be a robust biomarker of aging in humans (Chen et al., 2016). However, DNA methylation is tissue/organ specific (Horvath et al., 2015). For a live person, DNA methylation-based BA could only be obtained from blood or saliva samples (Horvath et al., 2016). Many aspects of the human body would not be covered.



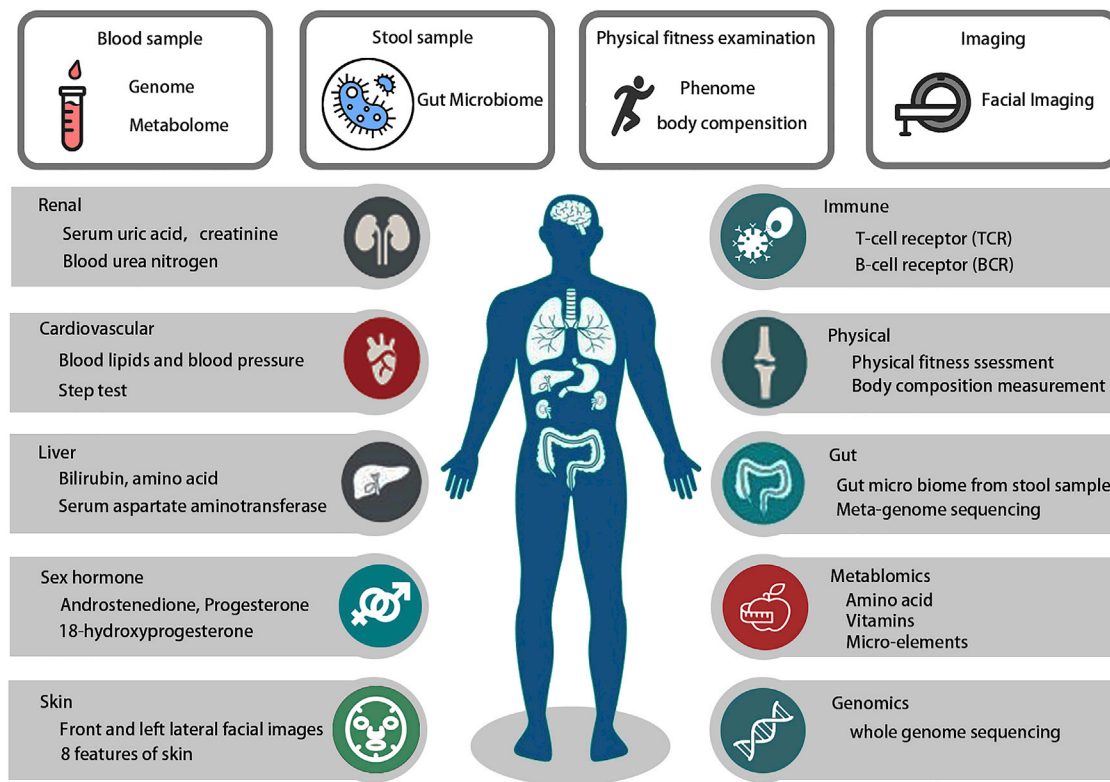


Figure 1. Multi-omics data were collected through different technologies and classified into groups of organs and systems

Multi-omics data from blood sample, stool sample, physical fitness examinations, and clinical images. In total, 403 features for each individual were measured. These were classified into nine categories, namely cardiovascular related, renal related, liver related, sex hormone, facial skin features, nutrition metabolism features, immune related, physical fitness related, and gut microbiome.

Recently, the concept of “deep phenotyping,” which aims to gather more specific details for the health status evaluation of precise medical areas, has emerged (Delude, 2015). The multi-omics approach provides such detailed information and offers the opportunity to explore multiple systems. Therefore, in the present study we established a cohort of young adults with multi-omics data, including gut microbiome, immune repertoire, metabolomics, blood chemicals, body composition, and phenomics (e.g., physical fitness test, facial skin scan). We used KDM to construct BAs of different organ/systems to investigate their commonalities and differences in terms of aging rates. We also demonstrated several applications of BAs, including utilizing BAs as phenotypes in genome-wide association studies (GWASs) and constructing polygenic risk scores (PRSs) of the aging rates of organs and systems in a dataset with 2,178 centenarians and 2,299 middle-aged individuals from the Chinese Longitudinal Healthy Longevity Survey (CLHLS) cohort.

RESULTS

Biological age of organs or systems constructed from multi-omics data

A total of 4,066 volunteers (48% males) aged between 20 and 45 years from the Shenzhen local area were recruited. Written informed consent was obtained from each individual. Multi-

omics level data were generated from blood sample, stool sample, physical fitness examination, and facial skin images (Figure 1). In total 403 features were measured, including 74 metabolomic features, 34 clinical biochemistry features, 36 immune repertoire features, 15 body composition features, 8 physical fitness features, 10 electroencephalography (EGG) features, 16 facial skin features, and 210 gut microbiome features (listed in Table S1). These were classified into nine categories, namely cardiovascular related, renal related, liver related, sex hormones, facial skin features, nutrition/metabolism features, immune related, physical fitness related, and gut microbiome.

After classification, the relationship with sex and age for each feature was examined. As we discovered that a large proportion of features had sex-specific effects (Figures 2A and 2B; Table S2), the following construction of BAs was conducted for male and female groups separately. Each feature was regressed into CA and only features significantly correlated with age ($p < 0.05$) were utilized for the generation of BAs. Moreover, features with redundant information were filtered out (see STAR methods). Finally nine BAs of different organs and systems were generated, and distinct patterns of correlations with chronological ages are shown in Figure 3. The cardiovascular age has the least variance among subjects while the variation in liver ages is quite large, indicating potential differences of aging effects for organs and systems.

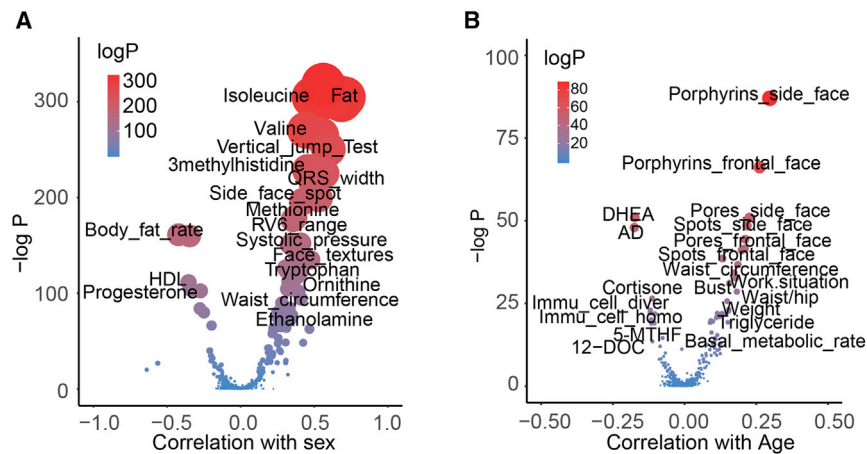


Figure 2. Changes in multi-omics features (A and B) Volcano plots representing changes in multi-omics features ($n = 403$) regarding sex (A) and age (B). Each feature from multi-omics tests was correlated with age and sex; the $-\log_{10}$ scale p-values from spearman correlation analysis were shown in the figure. We observed that a large proportion of features had sex-specific effects, therefore the constructions of biological ages were conducted for male and female groups separately.

Biological ages of different organs/systems show diverse correlations

To deeply study the characteristics of the aging processes of different organs and systems, we constructed an aging rate index, which took the difference between BA and CA and divided it by CA. This aging index represented the relative aging acceleration or deceleration per year. The pairwise correlations among multiple aging rate indexes were then assessed. The physical fitness age had generally high correlations with all other systems (Figure 4A). The BAs of the renal and sex hormone systems were the most correlated ($r = 0.53$). Sex hormone age was correlated with that of the renal ($r = 0.53$) and immune ($r = 0.44$) systems. Interestingly, the aging rate of the renal system was negatively correlated with that of gut microbiome ($r = -0.07$). The gut microbiota influences the actions of a range of xenobiotics in both beneficial and potentially harmful ways (Clarke et al., 2019), and it has been reported that the accumulation of microbiota-derived metabolites was associated with chronic kidney diseases (Joossens et al., 2019). The negative correlation could be caused by an increased diversity of conditional pathogenic bacteria leading to accumulation of toxic metabolites, thereby giving rise to disorders of the renal system (Wang et al., 2020). The positive counterpart of this situation is that the gut microbiome of centenarians and semi-supercentenarians who have escaped renal diseases is particularly suited for xenobiotic degradation (Rampelli et al., 2019). The diverse directions of correlations were consistent with the existence of multiple “clocks” throughout the whole body.

Individuals can be clustered according to characteristics of multiple biological ages

For each subject, the BAs of multiple organs and systems were constructed. Due to missing variables among individuals only 481 individuals had complete records, and nine biological aging rate indexes for these subjects were used for clustering analysis with the aim of identifying different aging patterns within the study population. The clustering result is shown in Figure 4B, with the color gradient representing the aging rates. Red indicates faster and blue indicates slower aging rates. The faster and slower rates are relative to the person’s CA; for instance if the BA is larger than the CA, the person is aging faster. Interestingly, individuals could be initially separated into two clusters.

The cluster above has an overall redder color while the cluster below shows relatively more blue colors; individuals in the cluster above are generally aging faster than the individuals in the cluster below with regard to all organs and systems. Within each cluster, subclusters were formed by the patterns of aging rates of different organs and systems. The subcluster at the bottom showed even more blue color, indicating that these people may have much slower aging rates. When comparing the clustering information with body mass index (BMI) (Figure 4B), it was found that overweight people (indicated by orange color in the right bar) were classified into different clusters representing different aging patterns. The two subclusters indicated by square right brackets in Figure 4B include relatively denser overweight people than others. These two subclusters are very different in terms of aging patterns, with the bottom one having much younger liver ages but older physical fitness ages. This may indicate that excess weight or obesity have different causes among individuals.

Determining BAs of different organs and systems may permit detailed evaluations of the source of specifically accelerated aging components in each individual. For instance, some overweight individuals have a faster aging rate in physical fitness and the nutrition metabolism system, while others have a faster aging rate for liver. This detailed information could potentially identify intervention targets for improving health status as well as slowing down the aging process.

Specific biological age measures predict diseases or phenotypes of corresponding organs

One of the ultimate objectives of constructing BA clocks is predicting abnormalities, disorders, and even mortality. To evaluate the predictive efficiency of BAs, we used the aging rate indexes to predict non-alcoholic fatty liver, which was the most common abnormality in our study sample. Logistic regressions were used for predictions. The results are shown in Figure 5. The severity of non-alcoholic fatty liver disease was associated with the liver aging index, which is consistent with our expectation that BAs could predict diseases or phenotypes of corresponding organs.

Evaluating biological ages of different organs/systems in the NHANES

We have used the same approach to classifying features into organs and systems for the dataset from the United States

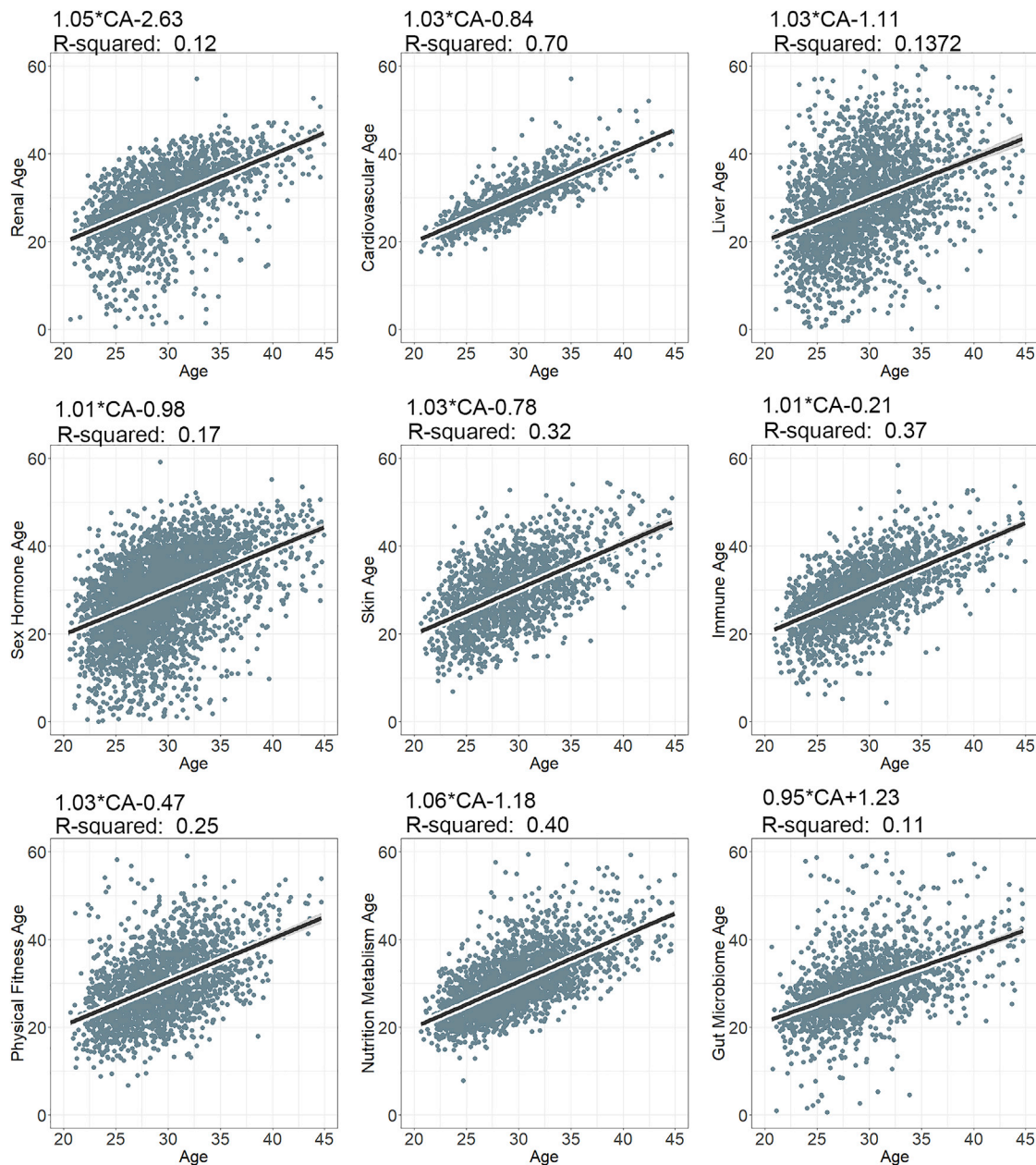


Figure 3. Relationships between biological ages and chronological age and their linear regression lines

Cardiovascular age has the highest explanation for chronological age. Gut microbiome age explained the least. Liver age and sex hormone age have high variations. The R-squared was the coefficient of determination calculated from linear regression model.

National Health and Nutrition Examination Survey (NHANES) between 1999 and 2012. Mortality follow-up was based on linked data from records taken from the National Death Index through 2016. After excluding individuals younger than 18 years, people died from infectious diseases and accidents as well as entries with missing features. Three BAs, namely cardiovascular age, liver age, and renal age, were calculated in 3,868 individuals. Among these, 625 individuals were deceased, among whom 128 subjects died of heart disease. The features

we used for constructing the BAs are listed in Table S3. We then used Cox proportional hazard models to investigate which ones have more predictive power for mortality. The models were adjusted for sex and CA. First, we compared the predicting power between BA and single features. Total cholesterol, blood glucose, lipoprotein, blood pressure, and CA significantly predicted mortality caused by heart disease. By combining these markers and constructing a BA of the cardiovascular system, the prediction power was significantly boosted (Figure 6A).

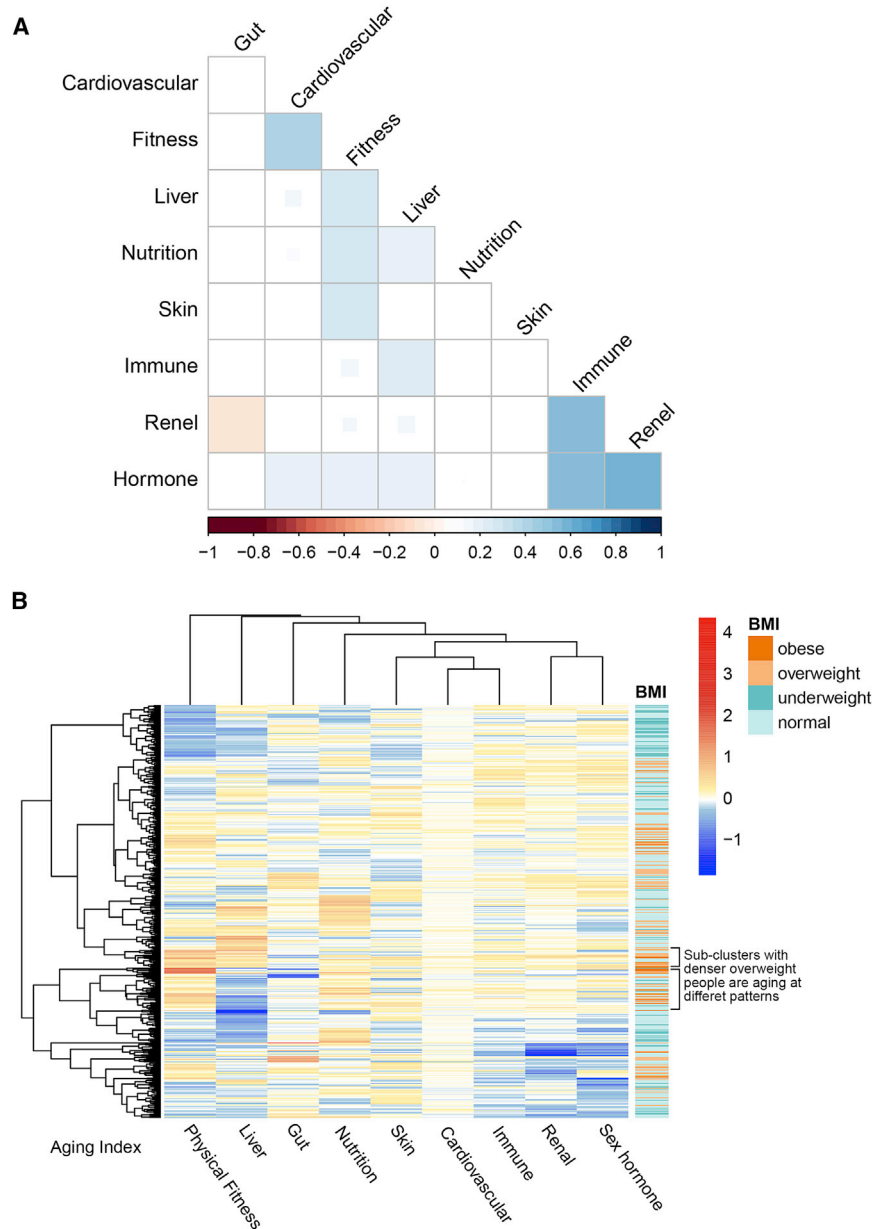


Figure 4. Clustering individuals using biological ages identified different patterns of being overweight

(A) Heatmap of pairwise correlations among aging indexes of multiple organs and systems. The color gradient represents the correlation coefficients from a Spearman correlation. Blue indicates positive correlations and red indicates negative correlations.

(B) Clustering heatmap of 481 individuals according to different biological ages. The color gradient represents the aging rates. Red indicates faster and blue indicates slower aging rates. Faster and slower are relative to the person's chronological age; for instance, if the biological age is larger than his chronological age, the person is aging faster.

Distinct genetic architectures of multiple organs' and systems' aging rates

Using a multi-omics dataset, we have assessed the aging rates of different organs or systems, identifying their similarities and differences. Next, we determined whether the differences could be explained by genetic factors. We compared the genetic architectures of the aging rate indexes of multiple systems. Using these aging rate indexes as phenotypes, GWASs were performed.

After standard GWAS quality control processes, 7,236,472 common SNPs were identified. The results suggest distinct genetic architectures among these systems. Additionally, we summarized the GWAS signal densities for each association, with the number of signals ($p < 0.05$) per 10-Mbp window on the genome calculated and plotted (Figure 7A.). Interestingly, the signal densities of each system or organ are versatile (Figure 7A), but one region was identified to be correlated with aging in all organs/systems. This region harbors the major histo-

compatibility complex on chromosome 6, indicating the potential importance of the immune system in aging processes. The Manhattan plots for GWAS are shown in Figures S1–S9.

To further investigate biological functions associated with biological aging rate indexes and improve the power of genetic studies by reducing the number of statistical tests, we employed pathway-based association (see STAR methods). The identified ($p < 0.05$) pathways are shown in Figure 7B. The nucleotide excision repair (NER) pathway was identified in five systems. Another two pathways related to DNA repair, base excision repair, and non-homologous end-joining pathways were also identified in aging of the cardiovascular system. Many studies have reported that a defective

This suggested that individual markers had independent contributing effects to cardiovascular diseases. Second, we compared the predictive power of the BA of different organs. The predictive power for mortality in the biological aging index was significantly higher than that of CA (Figures 6B and 2C). When predicting death caused by heart disease, the cardiovascular aging rate performed better than liver and renal aging indexes (Figure 6C). This result suggested that classifying features to construct organ/system-specific BA could gain more specific power in terms of predicting organ-related disease mortality. If the cause of death is not specified, combining all features together for an integrated BA would be an improvement (Figure 6B).

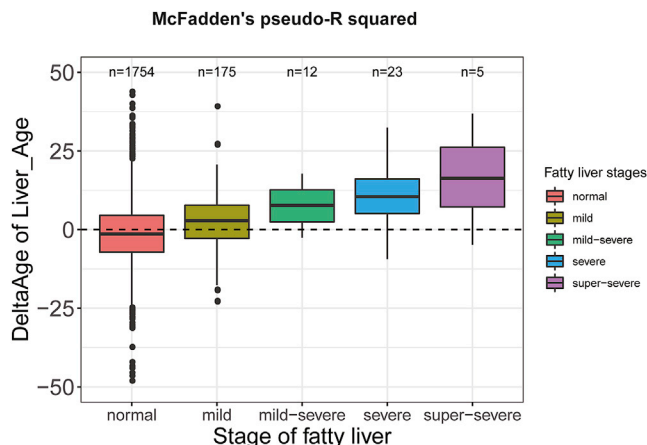


Figure 5. Predicting non-alcoholic fatty liver using biological age
Older liver age is associated with non-alcoholic fatty liver. The pseudo-R-squared was calculated from logistic regression using McFadden's method.

NER gene would cause instability of DNA and thereby accelerate aging (Chen et al., 2020; Martejn et al., 2014; Nieldernhofer et al., 2018). Several signaling pathways correlated with aging were also identified, including p53, Hedgehog, PPAR, insulin, VEGF, and Notch signaling pathways. It is believed that changes and damage occurring at the cellular level play a causative role in aging (Tabibzadeh, 2021). These signaling pathways participated in maintaining cellular homeostasis and health. All pathways significantly associated with biological aging rates are listed in Table S4.

Polygenic scores of biological ages can predict longevity

Another application of BAs is forecasting an individual's mortality. Using the effects of SNPs as a bridge, we have constructed PRSs (see STAR methods) of different organs and systems in the CLHLS cohort, including 2,178 centenarians and 2,299 middle-aged controls (Zeng et al., 2016). The polygenic scores were used, individually and jointly, to classify centenarians and middle-aged individuals. The PRS for skin aging index significantly predicted longevity after correction for multiple testing ($p = 9.3 \times 10^{-4}$, $p < 0.05/9$). Other PRSs predicted longevity at a nominally significant level ($p < 0.05$) (Figure 7C). While incorporating all the aging polygenic scores to predict whether a person could be centenarian, we also achieved significant prediction (area under the curve 95% confidence interval [0.514, 0.586]). However, this was not an exceptional prediction. The possible reasons could be (1) that there is missing heritability of longevity which has not been identified by current GWAS, or (2) that many environmental factors, lifestyles, and the gene-environment interactions are influencing longevity. Therefore, using only PRS for longevity prediction was able to obtain only limited prediction efficiency.

DISCUSSION

Our study revealed evidence that there might be multiple "clocks" within the whole-body system. We have utilized multi-

omics data, including clinical tests, metabolomes, proteomes, microbiomes, physical fitness examinations, and facial skin examinations, to estimate the BAs of different organs (e.g., liver and kidney) and systems (e.g., immune systems and metabolic system). The results showed distinctions of the aging rates of organs and systems. These BAs could be applied for clustering individuals and identifying the sources of age-related dysfunction. In addition, we have performed GWASs using each respective biological aging index and have compared the differences in genetic architectures among different organs and systems. Pathways-based association analyses demonstrated relevance between biological functions and aging. Last but not least, we utilized the GWAS results of BAs to construct PRSs in the CLHLS cohort to enable evaluation of the genetic correlations between systems' aging and longevity.

Although aging is a lifelong process (Kuh et al., 2014), most human aging studies were conducted in older populations or cohorts with a high incidence of chronic diseases. Some studies reported that age-related changes could be detected from the early 20s (Akima et al., 2001), and the aging process in young healthy adults is still largely unknown. In addition, the organs of young adults are not yet heavily damaged, offering the possibility to prevent age-related diseases. Accordingly, we have chosen to establish a young cohort aged between 20 and 45 years with the aim of studying the early changes of aging.

The biomarker selection process is essential for BA construction, and many approaches have been implemented. Our study utilizes a very large number of biomarkers that comprehensively cover most systems of the human body in the same dataset for studying multi-system BAs. We have collected as many biomarkers as possible from multi-omics approaches and have performed systematic evaluations of each measurement. Statistical analyses were used to calculate the aging effects of every biomarker, and redundant biomarkers were excluded. The informative markers were then classified into organs and systems according to existing biological knowledge.

On the whole, the results of our approach suggest that there might be systemic aging drivers/clocks overlaid with organ/tissue-specific counterparts. The pairwise correlations among multiple BAs showed that the physical fitness age has a generally high correlation with all other systems, and the correlation directions are diverse. These distinctions of aging rates appear to have a genetic basis. The overall p value distribution of GWASs across the genome was different between the renal system and hormonal as well as nutrition/metabolic systems. Pathway-based associations revealed different correlated pathways. Most identified pathways were functionally related to the corresponding organ.

At variance with existing studies which integrated multiple biomarkers into one BA (in turn correlated with disease status and behaviors) without considering differences between organs and systems (Wilmanski et al., 2019), our study provides a more detailed evaluation of aging for different functional systems. Identifying abnormalities of one particular organ or system may lead to a specifically targeted treatment. Our liver age predicts the clinically diagnosed severity of fatty liver disease. The biomarkers we used to construct liver age are all from blood samples, and the use of liver age to scan the population would

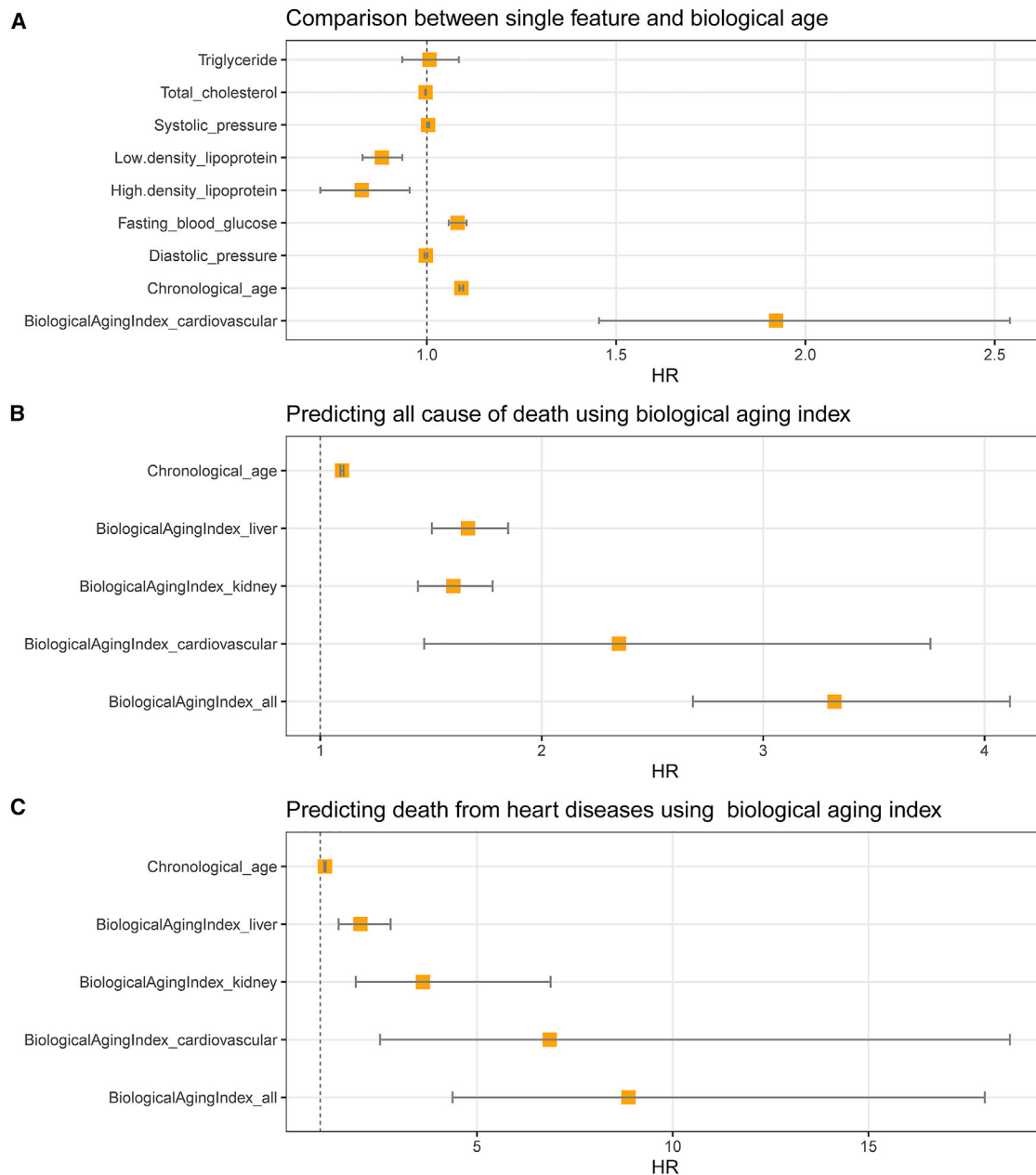


Figure 6. Predicting mortality in NHANES data

While constructing biological ages in NHANES data, cardiovascular age, liver age, and renal age could predict mortality.

(A) Results of Cox proportional hazard model comparing single features and biological age.

(B) Results of Cox proportional hazard model predicting all causes of mortality.

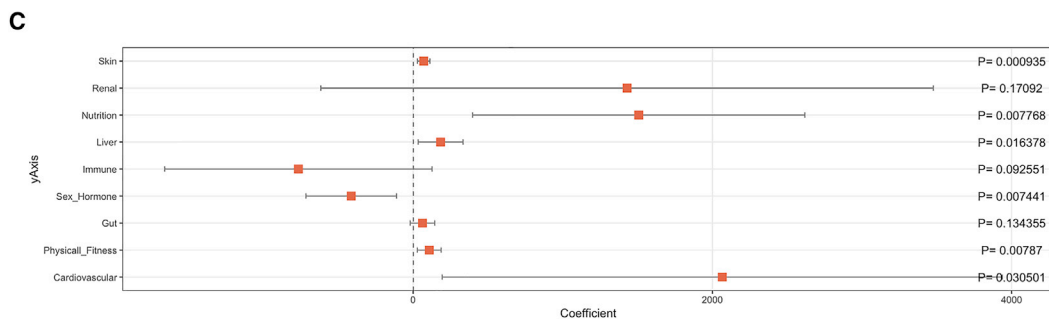
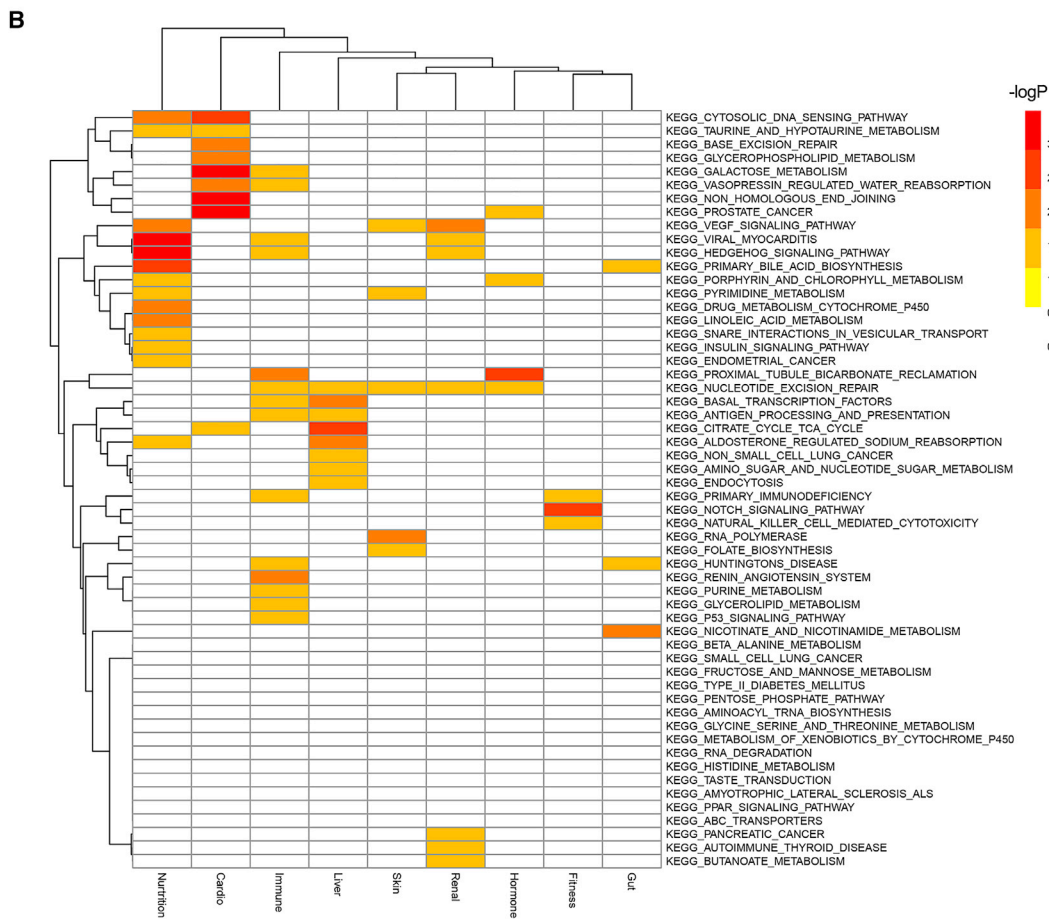
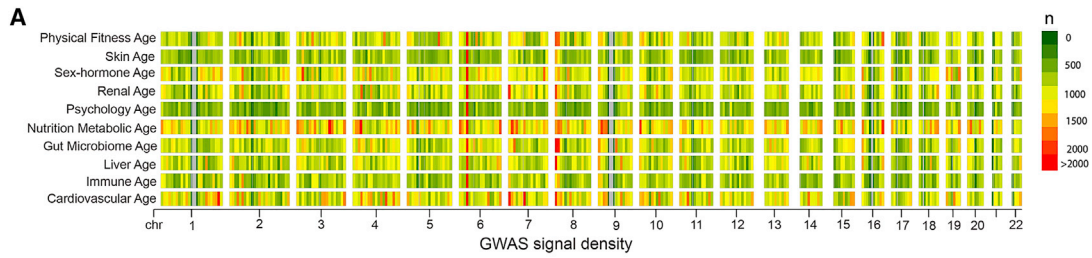
(C) Results of Cox proportional hazard model predicting mortality caused by heart diseases.

HR, hazard ratio. The error bar represents a 95% confidence interval of HR.

be cost-effective and could identify liver abnormalities at an early stage.

A recent multi-omics study has mentioned the concept of “ageotypes” while using 608 multi-omics features for clustering analyses. The results showed that those features were enriched into four aging-related types, namely immunity, metabolic, liver dysregulation, and kidney dysregulation (Ahadi et al., 2020).

Their data showed hints at organs and systems differences in terms of aging; however, their analyses only included 106 individuals and many aspects of human body function were not evaluated. In this regard, our study covers more aspects, such as the cardiovascular system, skin, and sex hormones, in a much larger cohort. Moreover, in the present study we also provided genetic evidence of the existence of “ageotypes.” There are studies that



(legend on next page)

have developed DNA methylation ages for multiple tissues (Horvath, 2013), supporting the multiple “clocks” hypothesis. However, from a translational perspective, DNA methylation data of multiple tissues will be very difficult to obtain in a live person. Furthermore, tissues and organs/systems are quite different. Tissues usually consist of homogeneous cell types, and the variations within a tissue are usually small, whereas organs consist of multiple tissues, for example muscle and fibrous tissues in the heart.

One possible explanation for these different aging rates could be that the aging process occurs in every cell of the whole body, and the different composition of cell types within the organs will lead to distinct aging rates. Moreover, cell type differentiation is decided by genetics, especially by the pattern of transcription factor expression (Almalki and Agrawal, 2016). Therefore, there might be one centralized driver/clock controlling the aging of the cell, the basic functional unit of the body. Meanwhile, the organizations of cell populations drive the aging process of different organs and systems. The physical fitness age, constructed using mostly muscle and fat tissue quantifications, as well as the power and strength of muscles, is an example of how we addressed the complexity of the underpinning biology of such a complex trait. Muscle tissue is involved in almost all organs (Jaslove and Nelson, 2018) and, hence, the BA of physical fitness is correlated with most other BAs. This result is consistent with available knowledge, the physical fitness assessment being the most widely used general evaluation of health and aging status. A single measure of BMI could provide information about a person’s health and aging status (Lee et al., 2017), but this single measurement is lacking in resolution as it only provides a general qualitative evaluation.

At present, to a person who is aging faster than average, one can hardly tell which part of the body is abnormal and how to improve it. Our comprehensive evaluations of the aging rates using multi-omics biomarkers could provide more detailed information, not only on which part of the body is dysfunctional but also to specifically suggest gene- or pathway-targeted interventions/drugs. For single interventions shown to affect lifespan and healthspan, it is unlikely that a single intervention will work in every individual even if the median lifespan of the population is affected. In these cases, there may be relationships between the response of an individual and the rate of aging of different “clocks,” allowing for better prediction of responders and non-responders.

We have used our BAs to predict disease status as well as longevity. Most previous studies have used BAs to predict mortality (Hastings et al., 2019; Jee, 2019). Since our BAs improved resolution at organ and system levels, we have found that certain BAs could predict tissue-related disease better than other BAs. For instance, cardiovascular age could predict mortality caused by heart disease better than liver and renal ages in

an independent NHANES dataset. On the other hand, we have constructed PRSs using the SNP effects estimated in our datasets from the CLHLS (Zeng et al., 2016), which includes 2,178 centenarians and 2,299 middle-aged controls. The results showed that some PRSs could significantly predict longevity, proving the existence of a genetic correlation between aging processes and longevity and suggesting that a biological aging index can be used as phenotype for the genetic studies of longevity. We predict that by using the organs’ BAs coupled to genetic studies of longevity, resolution could also be improved at the whole-body level as well as within biological units/organs/systems.

Our approaches to estimating BAs for organs and systems could be easily used in clinical practice or health management for elderly people. It is noteworthy that the biomarkers we used for constructing BAs were mostly gained from routine physical checkups or blood sample tests, which are easy to scale up for health management of larger populations.

Limitations of the study

Some limitations of the current study need to be acknowledged. First, this study is based on a cross-sectional dataset in which we can only identify associations rather than causalities. Future follow-up studies are required to validate our findings. Second, the multi-omics features were classified manually according to their clinical interpretations or data types, and overlapping was avoided between classes to study the differences of organs and systems. This method ignored the interactions among organs and systems. Future studies using unsupervised approaches for classifying the features and studying the interactions between systems are required. Third, the relatively small sample size limited the power of the GWAS. We only gained suggestive signals from variant-based association. We utilized pathway-based association to improve GWAS power by leveraging on biological knowledge. Finally, the aging process is complex, being influenced by genetics, environment, and their interactions. This might be the reason why we only gained limited efficiency while using PRSs to predict longevity phenotypes. Gene-environment interactions are important avenues to be studied.

STAR★METHODS

Detailed methods are provided in the online version of this paper and include the following:

- KEY RESOURCES TABLE
- RESOURCE AVAILABILITY
 - Lead contact
 - Materials availability
 - Data and code availability

Figure 7. Distinct genetic architectures of different biological ages

(A) GWAS signal densities for each association. The number of signals ($p < 0.05$) per 10M window on the genome were calculated and plotted. The p values were calculated by PLINK from linear regression model; $-\log_{10}$ scale p values were used.
 (B) Pathways associated with different biological ages. The p values were calculated by FASTBAT from the χ^2 distribution.
 (C) Prediction efficiencies of polygenic risk scores of biological ages predicting longevity in CLHLS data. The p values were calculated from a logistic regression model.

- EXPERIMENTAL MODEL AND SUBJECT DETAILS
- QUANTIFICATION AND STATISTICAL ANALYSIS
- METHOD DETAILS

- Routine medical examination
- Physical fitness assessment
- Facial skin assessment
- Quantitative measurement of blood metabolites using mass spectrometry
- Whole genome sequencing sample recruitment and data processing
- Metagenomics sequencing
- Immune repertoire sequencing (IR-SEQ)
- Data quality control and biological ages constructions
- Biological age calculation and cox regression analysis in National Health and Nutrition Examination Survey (NHANES)
- Single variant-based association
- Set-based association
- Polygenic score risk prediction

SUPPLEMENTAL INFORMATION

Supplemental information can be found online at <https://doi.org/10.1016/j.celrep.2022.110459>.

ACKNOWLEDGMENTS

We acknowledge support from the National Key Research and Development Program of China (2020YFC2002902), the National Natural Science Foundation of China (no. 8194100278), the Technology and Innovation Commission of Shenzhen Municipality under grant no. JCYJ20170412153100794, and the Technology and Innovation Commission of Shenzhen Municipality under grant no. JCYJ20180507183615145.

AUTHOR CONTRIBUTIONS

Conceptualization, J.W., H.Y., X.X., C.N., and B.K.; investigation, Y.L., R.L., and C.N.; formal analysis, Y.L., R.L., Z.L., Z.H., and Y.W.; data curation, Y.L., Z.W., and J.D.; resources, R.W., Y.Z., Z.W., M.J., K.C., Y. Shi, J.G., T.L., and X.J.; visualization, Y.L., R.L., Y.Y., and D.Z.; writing – original draft, Y.L., C.N., and R.L.; writing – review & editing, Y.L., B.K., C.F., J.-D.J.H., and X.Z.; supervision, X.X., J.W., H.Y., and X.Z.; project administration, H.Z. and Y. Sun.

DECLARATION OF INTERESTS

The authors declare no competing interests.

Received: July 19, 2021

Revised: December 6, 2021

Accepted: February 8, 2022

Published: March 8, 2022

REFERENCES

Ahadi, S., Zhou, W., Rose, S.M.S.-F., Sailani, M.R., Contrepois, K., Avina, M., Ashland, M., Brunet, A., and Snyder, M. (2020). Personal aging markers and ageotypes revealed by deep longitudinal profiling. *Nat. Med.* 26, 83–90.

Akima, H., Kano, Y., Enomoto, Y., Ishizu, M., Okada, M., Oishi, Y., Katsuta, S., and Kuno, S. (2001). Muscle function in 164 men and women aged 20–84 yr. *Med. Sci. Sports Exerc.* 33, 220–226.

Almalki, S.G., and Agrawal, D.K. (2016). Key transcription factors in the differentiation of mesenchymal stem cells. *Differentiation* 92, 41–51.

Bae, C.-Y., Kang, Y.G., Kim, S., Cho, C., Kang, H.C., Yu, B.Y., Lee, S.-W., Cho, K.H., Lee, D.C., and Lee, K. (2008). Development of models for predicting biological age (BA) with physical, biochemical, and hormonal parameters. *Arch. Gerontol. Geriatr.* 47, 253–265.

Bakshi, A., Zhu, Z., Vinkhuyzen, A.A., Hill, W.D., McRae, A.F., Visscher, P.M., and Yang, J. (2016). Fast set-based association analysis using summary data from GWAS identifies novel gene loci for human complex traits. *Sci. Rep.* 6, 32894.

Balding, D.J. (2006). A tutorial on statistical methods for population association studies. *Nat. Rev. Genet.* 7, 781–791.

Chang, C.C., Chow, C.C., Tellier, L.C., Vattikuti, S., Purcell, S.M., and Lee, J.J. (2015). Second-generation PLINK: rising to the challenge of larger and richer datasets. *Gigascience* 4, 7.

Chen, B.H., Marioni, R.E., Colicino, E., Peters, M.J., Ward-Caviness, C.K., Tsai, P.-C., Roetker, N.S., Just, A.C., Demerath, E.W., and Guan, W. (2016). DNA methylation-based measures of biological age: meta-analysis predicting time to death. *Aging (N Y)* 8, 1844.

Chen, Y., Geng, A., Zhang, W., Qian, Z., Wan, X., Jiang, Y., and Mao, Z. (2020). Fight to the bitter end: DNA repair and aging. *Ageing Res. Rev.* 64, 101154.

Cho, I.H., Park, K.S., and Lim, C.J. (2010). An empirical comparative study on biological age estimation algorithms with an application of Work Ability Index (WAI). *Mech. Ageing Dev.* 131, 69–78.

Choi, S.W., and O'Reilly, P.F. (2019). PRSice-2: polygenic risk score software for biobank-scale data. *Gigascience* 8, giz082.

Clarke, G., Sandhu, K.V., Griffin, B.T., Dinan, T.G., Cryan, J.F., and Hyland, N.P. (2019). Gut reactions: breaking down xenobiotic–microbiome interactions. *Pharmacol. Rev.* 71, 198–224.

Comfort, A. (1969). Test-battery to measure ageing-rate in man. *Lancet* 294, 1411–1415.

De Maesschalck, R., Jouan-Rimbaud, D., and Massart, D.L. (2000). The mahalanobis distance. *Chemometrics Intell. Lab. Syst.* 50, 1–18.

Delude, C.M. (2015). Deep phenotyping: the details of disease. *Nature* 527, S14–S15.

Dubina, T., Mints, A.Y., and Zhuk, E. (1984). Biological age and its estimation. III. Introduction of a correction to the multiple regression model of biological age and assessment of biological age in cross-sectional and longitudinal studies. *Exp. Gerontol.* 19, 133–143.

Franceschi, C., Garagnani, P., Parini, P., Giuliani, C., and Santoro, A. (2018). Inflammaging: a new immune–metabolic viewpoint for age-related diseases. *Nat. Rev. Endocrinol.* 14, 576–590.

Harman, D. (1991). The aging process: major risk factor for disease and death. *Proc. Natl. Acad. Sci. U S A* 88, 5360–5363.

Hastings, W.J., Shalev, I., and Belsky, D.W. (2019). Comparability of biological aging measures in the national health and nutrition examination study, 1999–2002. *Psychoneuroendocrinology* 106, 171–178.

Hofecker, G., Skalicky, M., Kment, A., and Niedermüller, H. (1980). Models of the biological age of the rat. I. A factor model of age parameters. *Mech. Ageing Dev.* 14, 345–359.

Hollingsworth, J.W., Hashizume, A., and Jablon, S. (1965). Correlations between tests of aging in Hiroshima subjects—an attempt to define "physiologic age". *Yale J. Biol. Med.* 38, 11.

Horvath, S. (2013). DNA methylation age of human tissues and cell types. *Genome Biol.* 14, 1–20.

Horvath, S., Garagnani, P., Bacalini, M.G., Pirazzini, C., Salvioli, S., Gentilini, D., Di Blasio, A.M., Giuliani, C., Tung, S., and Vinters, H.V. (2015). Accelerated epigenetic aging in down syndrome. *Aging Cell* 14, 491–495.

Horvath, S., Gurven, M., Levine, M.E., Trumble, B.C., Kaplan, H., Allayee, H., Ritz, B.R., Chen, B., Lu, A.T., and Rickabaugh, T.M. (2016). An epigenetic clock analysis of race/ethnicity, sex, and coronary heart disease. *Genome Biol.* 17, 1–23.

Horvath, S., and Raj, K. (2018). DNA methylation-based biomarkers and the epigenetic clock theory of ageing. *Nat. Rev. Genet.* 19, 371–384.

- Jaslove, J.M., and Nelson, C.M. (2018). Smooth muscle: a stiff sculptor of epithelial shapes. *Philos. Trans. R. Soc. B: Biol. Sci.* **373**, 20170318.
- Jee, H. (2019). Selection of a set of biomarkers and comparisons of biological age estimation models for Korean men. *J. Exerc. Rehabil.* **15**, 31.
- Joossens, M., Faust, K., Gryp, T., Nguyen, A.T.L., Wang, J., Eloit, S., Schepers, E., Dhondt, A., Pletinck, A., and Vieira-Silva, S. (2019). Gut microbiota dynamics and uraemic toxins: one size does not fit all. *Gut* **68**, 2257–2260.
- Klemera, P., and Doubal, S. (2006). A new approach to the concept and computation of biological age. *Mech. Ageing Dev.* **127**, 240–248.
- Kröll, J., and Saxtrup, O. (2000). On the use of regression analysis for the estimation of human biological age. *Biogerontology* **1**, 363–368.
- Kuh, D., Karunanathan, S., Bergman, H., and Cooper, R. (2014). A life-course approach to healthy ageing: maintaining physical capability. *Proc. Nutr. Soc.* **73**, 237–248.
- Lee, G., Park, J., Oh, S.-W., Joh, H.-K., Hwang, S.-S., Kim, J., and Park, D. (2017). Association between body mass index and quality of life in elderly people over 60 years of age. *Korean J. Fam. Med.* **38**, 181.
- Lehallier, B., Gate, D., Schaum, N., Nanasi, T., Lee, S.E., Yousef, H., Losada, P.M., Berdnik, D., Keller, A., and Verghese, J. (2019). Undulating changes in human plasma proteome profiles across the lifespan. *Nat. Med.* **25**, 1843–1850.
- Levine, M.E. (2013). Modeling the rate of senescence: can estimated biological age predict mortality more accurately than chronological age? *J. Gerontol. Biol. Med. Sci.* **68**, 667–674.
- Li, H., and Durbin, R. (2009). Fast and accurate short read alignment with Burrows–Wheeler transform. *Bioinformatics* **25**, 1754–1760.
- Li, J., Jia, H., Cai, X., Zhong, H., Feng, Q., Sunagawa, S., Arumugam, M., Kultima, J.R., Prifti, E., and Nielsen, T. (2014). An integrated catalog of reference genes in the human gut microbiome. *Nat. Biotechnol.* **32**, 834–841.
- Li, R., Yu, C., Li, Y., Lam, T.-W., Yiu, S.-M., Kristiansen, K., and Wang, J. (2009). SOAP2: an improved ultrafast tool for short read alignment. *Bioinformatics* **25**, 1966–1967.
- Liberti, L., Lator, C., Maculan, N., and Mucherino, A. (2014). Euclidean distance geometry and applications. *SIAM Rev.* **56**, 3–69.
- Marteijn, J.A., Lans, H., Vermeulen, W., and Hoeijmakers, J.H. (2014). Understanding nucleotide excision repair and its roles in cancer and ageing. *Nat. Rev. Mol. Cell Biol.* **15**, 465–481.
- McFadden, D. (1979). *Quantitative Methods for Analysing Travel Behaviour of Individuals: Some Recent Developments* (Routledge).
- McKenna, A., Hanna, M., Banks, E., Sivachenko, A., Cibulskis, K., Kernytsky, A., Garimella, K., Altshuler, D., Gabriel, S., and Daly, M. (2010). The Genome Analysis Toolkit: a MapReduce framework for analyzing next-generation DNA sequencing data. *Genome Res.* **20**, 1297–1303.
- Nakamura, E., and Miyao, K. (2007). A method for identifying biomarkers of aging and constructing an index of biological age in humans. *J. Gerontol. Biol. Med. Sci.* **62**, 1096–1105.
- Nakamura, E., Miyao, K., and Ozeki, T. (1988). Assessment of biological age by principal component analysis. *Mech. Ageing Dev.* **46**, 1–18.
- Neale, B.M., and Sham, P.C. (2004). The future of association studies: gene-based analysis and replication. *Am. J. Hum. Genet.* **75**, 353–362.
- Niedernhofer, L.J., Gurkar, A.U., Wang, Y., Vijg, J., Hoeijmakers, J.H., and Robbins, P.D. (2018). Nuclear genomic instability and aging. *Annu. Rev. Biochem.* **87**, 295–322.
- Rampelli, S., Soverini, M., D’Amico, F., Barone, M., Tavella, T., Monti, D., Capri, M., Astolfi, A., Brigidi, P., and Biagi, E. (2019). Shotgun metagenomics of human gut microbiota up to extreme longevity and the increasing role of xenobiotics degradation. *mSystems* **5**, e00124.
- Stegeman, R., and Weake, V. (2017). Transcriptional signatures of aging. *J. Mol. Biol.* **429**, 2427–2437.
- Tabibzadeh, S. (2021). Signaling pathways and effectors of aging. *Growth* **3**, 53.
- Truong, D.T., Franzosa, E.A., Tickle, T.L., Scholz, M., Weingart, G., Pasolli, E., Tett, A., Huttenhower, C., and Segata, N. (2015). MetaPhlan2 for enhanced metagenomic taxonomic profiling. *Nat. Methods* **12**, 902–903.
- Wallach, J.B. (2007). *Interpretation of Diagnostic Tests* (Lippincott Williams & Wilkins).
- Wang, X., Yang, S., Li, S., Zhao, L., Hao, Y., Qin, J., Zhang, L., Zhang, C., Bian, W., and Zuo, L. (2020). Aberrant gut microbiota alters host metabolome and impacts renal failure in humans and rodents. *Gut* **69**, 2131–2142.
- Wilmanski, T., Rappaport, N., Earls, J.C., Magis, A.T., Manor, O., Lovejoy, J., Omenn, G.S., Hood, L., Gibbons, S.M., and Price, N.D. (2019). Blood metabolome predicts gut microbiome α -diversity in humans. *Nat. Biotechnol.* **37**, 1217–1228.
- Zeng, Y., Nie, C., Min, J., Liu, X., Li, M., Chen, H., Xu, H., Wang, M., Ni, T., and Li, Y. (2016). Novel loci and pathways significantly associated with longevity. *Sci. Rep.* **6**, 1–13.
- Zhang, W., Du, Y., Su, Z., Wang, C., Zeng, X., Zhang, R., Hong, X., Nie, C., Wu, J., and Cao, H. (2015). IMonitor: a robust pipeline for TCR and BCR repertoire analysis. *Genetics* **201**, 459–472.

STAR★METHODS

KEY RESOURCES TABLE

REAGENT or RESOURCE	SOURCE	IDENTIFIER
Biological samples		
EDTA-plasma and PBMCs prepared from intravenous whole blood collection	This paper	N/A
Fresh stool samples	This paper	N/A
Deposited data		
Summary statistics of associations between biomarkers and age	This paper	Mendeley Data: https://doi.org/10.6084/m9.figshare.19085156
National Health and Nutrition Examination Survey (NHANES) between 1999 and 2012	public data	NHANES, RRID:SCR_013201
Genetic data of Centenarians and young controls	Zeng et al., 2016 ; zengyi@nsd.pku.edu.cn	N/A
Software and algorithms		
Klemera and Doudal algorithm	Klemera and Doudal, 2006	https://doi.org/10.1016/j.mad.2005.10.004
Picard/BWA/GATK pipeline	Li and Durbin, 2009 ; McKenna et al., 2010	GATK, RRID:SCR_001876
MetaHIT protocol	Metagenomics of the Human Intestinal Tract (MethIT) project	https://cordis.europa.eu/project/id/201052/reporting
IMonitor:Pipeline for TCR and BCR Repertoire Analysis	Zhang et al., 2015	https://pubmed.ncbi.nlm.nih.gov/26297338/
PRSice-2: Polygenic Risk Score software	Choi and O'Reilly, 2019	PRSice, RRID:SCR_017057
R scripts we used for calculating biological ages and performing statistical analyses	This paper	Database: https://doi.org/10.5281/zenodo.6002321

RESOURCE AVAILABILITY

Lead contact

Further information and requests for resources and reagents should be directed to and will be fulfilled by the Lead Contact, Xun Xu (xuxun@genomics.cn).

Materials availability

This study did not generate new unique reagents.

Data and code availability

- The summary statistics that support the findings of this study, including the associations between biomarkers and age are publicly available. DOIs are listed in the [key resources table](#). Individual-level data including genetic variants and clinical data will be shared by the lead contact upon request. Access to individual-level data is subject to the policies and approvals from the Human Genetic Resource Administration, Ministry of Science and Technology of the People's Republic of China.
- All original code has been deposited at Zenodo and is publicly available as of the date of publication. DOIs are listed in the [key resources table](#).
- Any additional information required to reanalyze the data reported in this work paper is available from the lead contact upon request.

EXPERIMENTAL MODEL AND SUBJECT DETAILS

This study has been approved and monitored by the Institutional Review Board at BGI-Shenzhen in conformance with WMA Declaration of Helsinki (2013). The approval number was BGI-IRB-20048. Posters and emails that advertising this study were posted at Yantian district, Shenzhen. Han Chinese volunteers, who have no major diseases that have occurred (such as acute infarction, end-stage renal edema, disability after stroke, cancer, paralysis) and no major transplantation and hematopoietic stem cell transplantation experience, aged from 20–45 years were recruited. The written form of consents was signed by each individual. Blood sample,

stool sample, physical fitness examinations as well as facial skin images were taken. The biological samples were taken by medical professionals in a local clinic. The sample dataset used in current study includes 4,066 individuals' records with mean age 29.42, ranging from age 20.49 to age 44.93. Among them, 1,957 (48%) are males and 2,109 (52%) are females. To ensure the safety of the volunteers' privacy, the data and samples were de-identified using a digital ID. The clinic stored the correspondence between patients' name and the digital ID. While the data analysts could only access the data with ID.

QUANTIFICATION AND STATISTICAL ANALYSIS

The statistical analysis relevant to biological age constructions and applications in this article were performed in R. The p values for spearman correlation tests in [Figures 2](#) and [4A](#) were calculated using student t-test. The R-squared in [Figure 3](#) was the coefficient of determination calculated from linear regression model. The pseudo R-squared in [Figure 5](#) was calculated from logistic regression using McFadden's method ([McFadden, 1979](#)). The hazard ratio (HR) in [Figure 6](#) were calculated from cox proportional hazards regression model, and its mean and 95% confidence interval were shown in the figure. The results of genetics association study shown in [Figure 7](#) was performed in PLINK ([Chang et al., 2015](#)) and FASTBAT ([Bakshi et al., 2016](#)). The p values for [Figure 7A](#) were calculated by PLINK from linear regression model. The p values for [Figures 7B](#) and [Table S4](#) were calculated by FASTBAT from χ^2 distribution. The p-values for [Figure 7C](#) were calculated from logistic regression model. There were no any methods that were used to check the distribution of our data, because we have selected non-parametric approaches for the data analyses, such as spearman correlation. The sample sizes for different omics data were diverse since many of the tests were optional to participants during sample collection. The sample sizes and features of each category are listed in [Table S5](#).

METHOD DETAILS

Routine medical examination

Routine medical examinations were carried out for everybody. A total of one urine tube and four blood tubes were collected. The blood tubes consisted of Na-Heparin Trace Element tubes, Serum Separator Tubes (SST), EDTA purple top tubes, and NMR black-top Lippitude. First morning void urine was collected in the yellow-top tube by participants the morning of their blood draw. In addition to biochemical tests, blood pressure, electrocardiogram, ultrasound examinations were performed. All clinical laboratory tests measured using Quest and Genova are listed in [Table S1](#).

Physical fitness assessment

Both health- and skill-related test components were included in the physical fitness assessment. The body compositions, including Body water, proteins, minerals, and body fat, were measured in InBody system utilizing bioelectrical impedance analysis. The cardiovascular endurance was measured through step tests and vital capacity. The muscular strength and endurance were assessed by pull-up for males and sit-up for females. For flexibility examinations, sit and reach test were conducted. High jump and hand grip test were conducted to measure the muscular strength of limbs. For skill related test, choice reaction time was examined.

Facial skin assessment

The skin features were measured using the VISIA® Complexion Analysis System. The photographic images were captured with standard, cross-polarized, parallel polarized, and ultraviolet light. Images were taken in two different close-up views (front and left lateral 37°) for each subject to quantify the scores for spots, wrinkles, pores, texture, and erythema.

Quantitative measurement of blood metabolites using mass spectrometry

The metabolites in blood were targeted and quantified using liquid chromatography coupled with triple quadrupole mass spectrometry (LC MS/MS), including ACQUITY UPLC I-Class (Waters) mounted with C18 column, Triple Quad 5500 (Sciex) and Xevo TQ-S (Waters). The MS/MS spectra corresponding to metabolites were acquired at positive ion mode with multiple reaction monitoring scans. The metal elements were measured by inductively coupled plasma mass spectrometry (ICP MS/MS), i.e. 7700x ICP-MS (Agilent). The mass spectra acquired were processed with MultiQuant (V. 3.0.2, Sciex) for amino acids, hormones and FSV, MassLynx (V. 4.1, Waters) for WSV and MassHunter (V. B.01.03, Agilent) for metal elements. The calibration curves were implemented with stable isotope-labeled compounds as internal standards. The accuracy of quality controls (QCs) with isotope-labeled IS was managed approximately every 15 samples to ensure the inter-batch stability. A total of the 81 out of the 84 metabolites were investigated for each individual.

Whole genome sequencing sample recruitment and data processing

The whole blood drawn from the participant vein was stored in the EDTA anticoagulant tubes to avoid hemolysis, while the plasma was obtained by centrifugation (3000 rpm, 10 min) and was preserved at -80°C until assay. The white cells were isolated for genomics DNA extraction. Whole-genome sequencing (WGS) to 30x were conducted for 1,553 subjects (Female N = 642, Male N = 911) from DNA in white cells using BGI-seq500. WGS data were aligned and variants called by the Picard/BWA ([Li and Durbin, 2009](#))/GATK ([McKenna et al., 2010](#)) pipeline. SNPs with mapping quality greater than 40, sequencing depth greater than 4, variant quality

greater than 2.0, Phred score of Fisher's test p value for strand bias smaller than 60.0, Haplotype score smaller than 13.0 and distance of alternative allele from the end of reads greater than 8.0 were kept for following analyses. We removed SNPs deviating from Hardy-Weinberg ($p < 1 \times 10^{-5}$), markers with more than 1% missing genotype data and variants with smaller than 1% minor allele frequencies. Individuals with heterozygosity greater than their standard deviations were excluded. One individual among relatives within 3rd degree of relationship was randomly selected to keep in the clean data set.

PCA were performed to investigate population stratification. No clear sub-cluster was observed. Typical north to south Grand aunt was demonstrated by the first principal component. Linear regression adding individual sex and top two principal components as covariates was performed for each SNP.

Metagenomics sequencing

Fresh stool samples were collected from recruited volunteers for metagenomics sequencing. The fecal DNA extractions were processed following the MetaHIT protocol, then Single-end metagenomics sequencing were performed using BGISEQ-500 platform. The low-quality reads were discarded, and the host DNA were removed based on human genome reference (hg38) by SOAP2 (Li et al., 2009) (version 2.22; identity ≥ 0.9). Taxonomic analysis was performed using MetaPhlan2 (Truong et al., 2015) following removal of human reads. The relative abundances of species were used in the current study. Meanwhile, the quality-controlled reads were mapped to integrated gene catalogue (IGC) (Li et al., 2014) by SOAP 2.22 (identity ≥ 0.95) to produce gene relative abundant profiles. Then, the abundances of genes within each KEGG pathway were aggregated to generate relative abundance profiles for functional modules.

Immune repertoire sequencing (IR-SEQ)

For human immune system, the enormous diversity of the T-cell receptor (TCR) and B cell receptor (BCR) repertoire is a good indicator for immune health status. We have performed deep targeted single-end sequencing for T-cell receptor (TCR) genes extracted from white cells and evaluated the immune status for each individual. Sequence data were analyzed using our previously developed pipeline, IMonitor (Zhang et al., 2015). Briefly, the reads were BLAST alignment onto V, D, J germline genes and alleles after basic quality control. Subsequently, a realignment for each result was performed with the aim of construct best gene sequences. Meanwhile, the base quality scores were recalibrated. Thirdly, the gene sequences were translated into amino acid to construct peptide sequences after a filtration of low abundance sequences (less than 5 supporting reads). Finally, the statistics of TCR of IGH data such as V-J pairing, V/J usage, CDR3 sequence frequency and CDR3 length distribution, were calculated.

Data quality control and biological ages constructions

Feature in which more than 100 samples had the zero values in microbiome data were excluded. As we identified a great proportion of features have sex different effects Figure 2A. The construction of biological ages was performed in male and female groups separately.

All the features were classified into organs and systems according to either clinical interpretations or data types. Features from clinical lab tests were classified according to the interpretation of blood chemical test (Wallach, 2007). The amino acids measures from the metabolic panel were classified into liver. The vitamin and microelements measures from metabolic panel were classified into nutrition metabolomic system. The microbiome features measured from stool sample were classified into gut. The facial imaging features were classified into skin. The T cell receptor gene features together with the blood cell count measures were classified into immune system. Features selected for each organ and system were listed in Table S1. As a result, 9 categories were classified.

The data quality control processes were performed in R 3.5.1. The multicollinearity of the features was further assessed using variance inflation factor (VIF). One of those features have redundant information (VIF >5) was kept for the construction of biological ages. As we also identified a great proportion of features have sex different effects. The construction of biological ages was performed in male and female groups separately.

The Euclidean distance (Liberti et al., 2014) and Mahalanobis distance (De Maesschalck et al., 2000) were used for outlier removals within each category. If the sample size is greater than number of biomarkers, we use Mahalanobis distance, otherwise, we use Euclidean distance. Individual data with either large Euclidean distance or large Mahalanobis distance ranking at top 5% were removed.

Each feature was regressed with age to evaluate their age effects using `lm()` function in R 3.5.1. Features significantly associated with age ($p < 0.05$) were kept for following study. The summary statistics of linear regression were listed in Table S2

Klemera and Doudal algorithm (Klemera and Doudal, 2006) was used for the construction of biological ages. Briefly, the KD method was consisted of two steps to convert those biomarkers into aging rate and making them comparable. The first step is regressing every biomarker to chronological age. By doing this, we gained the estimated age as well as its standard error using a particular biomarker. Every biomarker was processed and all the estimated ages have the unit 'year' which is the same as chronological age. We consider the regression step as a normalization process that make different markers comparable in terms of unit. The second step is aggregating the age estimates of each biomarker as well as chronological age and construct biological ages.

The statistical analyses of biological ages were performed in R 3.5.1. Pairwise spearman correlations were calculated by `cor()` function, correlation heatmap were generated by `corrplot()` function. The biological ages were normalized using inverse rank normal transformation method in `RNOmni()` function, and then unsupervised clustering were performed by K-means method and heatmap were generated by `pheatmap()` function.

Biological age calculation and cox regression analysis in National Health and Nutrition Examination Survey (NHANES)

We have matched features we used in the dataset from the National Health and Nutrition Examination Survey (NHANES) between 1999 and 2012. Mortality follow-up was based on linked data from records taken from the National Death Index through 2016. Those individuals younger than 18, people died from infectious diseases and accidents as well as samples with missing features were excluded. Three biological ages, including cardiovascular age, liver age, and renal age, were calculated. Then, we used cox proportional hazard models to investigate which one have more predictive power for mortality in R4.0.2 by `coxph()` function. The models were adjusted for sex and chronological age.

Single variant-based association

When phenotypes and genotypes have passed all the quality control processes, the basic analysis of genome-wide association were conducted. The single-locus statistical tests examined each SNP independently for association with the phenotypes (Balding, 2006; Chang et al., 2015). The types of statistical tests utilized mostly depends on the types of phenotypes. We have converted all constructed biological ages into normal distribution using inversed normal transformation in R 3.3.61. For continuous phenotype, linear regression is the most widely used method. All the association analyses were performed in PLINK1.9 (Chang et al., 2015). After association analyses, the coefficients of each SNPs for biological ages were gained. Pairwise Wilcoxon tests were used to test whether the distributions of SNP coefficients are different among biological ages.

Set-based association

The standard analysis of genome-wide association study uses single SNP marker as the test unit. However, due to small sample size, the complex LD structures and ethnic differences among different populations, many replication studies have failed. To improve GWAS power, the set-based association has been proposed during the initial development of GWAS (Neale and Sham, 2004). The set-based analysis combined the summary statistics of all variants within a putative biologically functional unit (coding region and possible regulatory region, genes within one pathway) to obtain a single p value that represents the significance of disease association of the gene. There are several benefits of using set-based association. Firstly, the gene is the functional unit of the human genome. Compared to genetic variants that have different allele frequencies, LD structure, and heterogeneity across diverse human populations, genes, and pathways are a highly conserved elements among different individuals. Therefore, set-based association analyses would lead to more consistent results across different ethnic populations.

For current study, FASTBAT was used for set-based association test. The test combined the p values of SNPs within one pathway (for each gene within the pathway, an extension of 10kb on each side as considering the regulatory region for the gene).

Polygenic score risk prediction

The validation in centenarian dataset were conducted through polygenic risk predictions. After genome-wide association analyses, each SNP would have effect (coefficients from linear regressions) on a particular biological age. Using these effects as weights to sum genotypes in centenarian dataset, a summed score will be formed for each individual (Choi and O'Reilly, 2019). This polygenic risk score has the biological meaning that it is the genetic components of one organ's/system's aging. Then each polygenic score of one organ/system was used as independent variables to predict whether a person is centenarian or not in generalized linear model using `glm()` function in R 3.6.1. In addition, all the polygenic scores of different organs/systems were aggregated in the same model to classify longevity groups using lasso regression.

Supplemental information

Distinct biological ages of organs and systems identified from a multi-omics study

Chao Nie, Yan Li, Rui Li, Yizhen Yan, Detao Zhang, Tao Li, Zhiming Li, Yuzhe Sun, Hefu Zhen, Jiahong Ding, Ziyun Wan, Jianping Gong, Yanfang Shi, Zhibo Huang, Yiran Wu, Kaiye Cai, Yang Zong, Zhen Wang, Rong Wang, Min Jian, Xin Jin, Jian Wang, Huanming Yang, Jing-Dong J. Han, Xiuqing Zhang, Claudio Franceschi, Brian K. Kennedy, and Xun Xu

Supplemental information

Distinct biological ages of organs and systems identified from a multi-omics study

Chao Nie, Yan Li, Rui Li, Yizhen Yan, Detao Zhang, Tao Li, Zhiming Li, Yuzhe Sun, Hefu Zhen, Jiahong Ding, Ziyun Wan, Jianping Gong, Yanfang Shi, Zhibo Huang, Yiran Wu, Kaiye Cai, Yang Zong, Zhen Wang, Rong Wang, Min Jian, Xin Jin, Jian Wang, Huanming Yang, Jing-Dong J. Han, Xiuqing Zhang, Claudio Franceschi, Brian K. Kennedy, Xun Xu

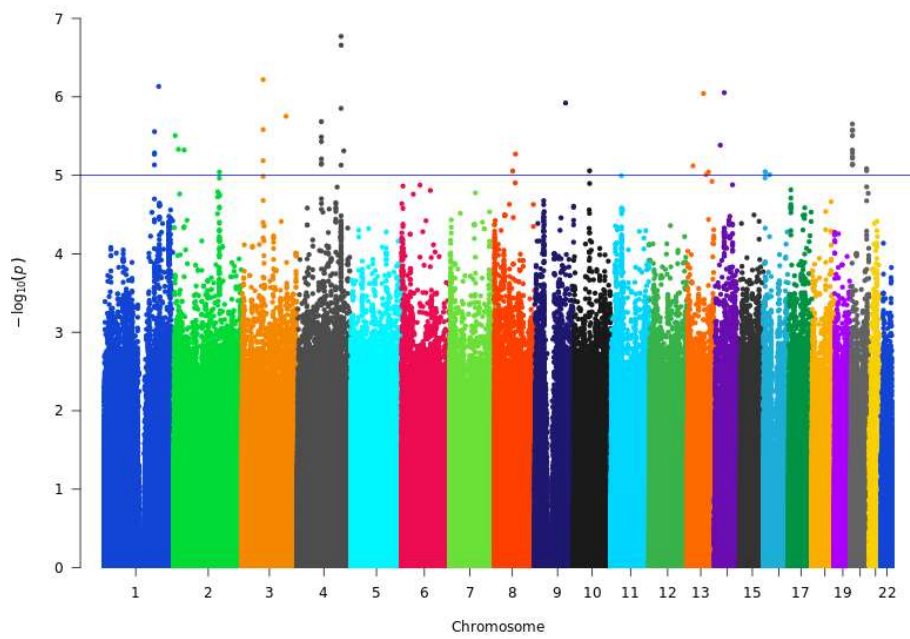


Figure S1. Manhattan plot of genome-wide association analysis for cardiovascular aging index, related to Figure 7A.

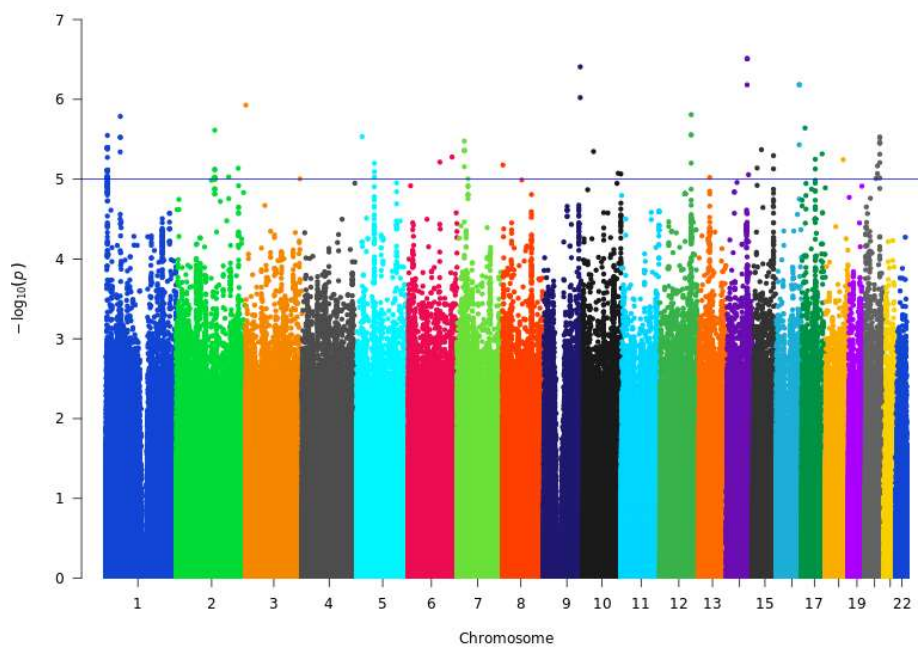


Figure S2. Manhattan plot of genome-wide association analysis for nutrition metabolism aging index, related to Figure 7A.

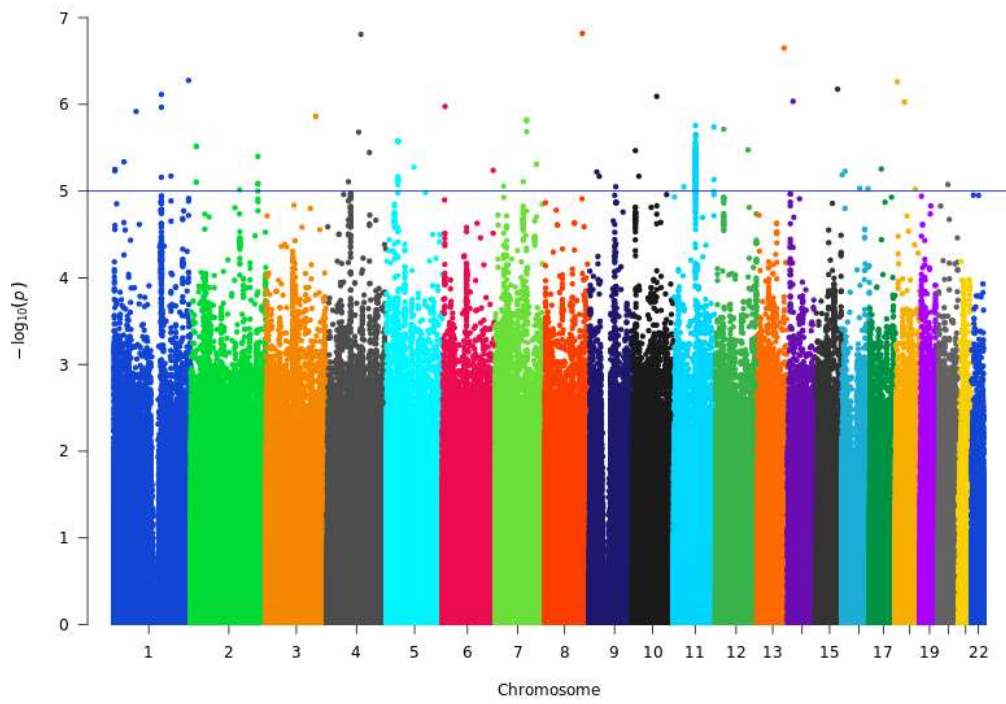


Figure S3. Manhattan plot of genome-wide association analysis for renal aging index, related to Figure 7A.

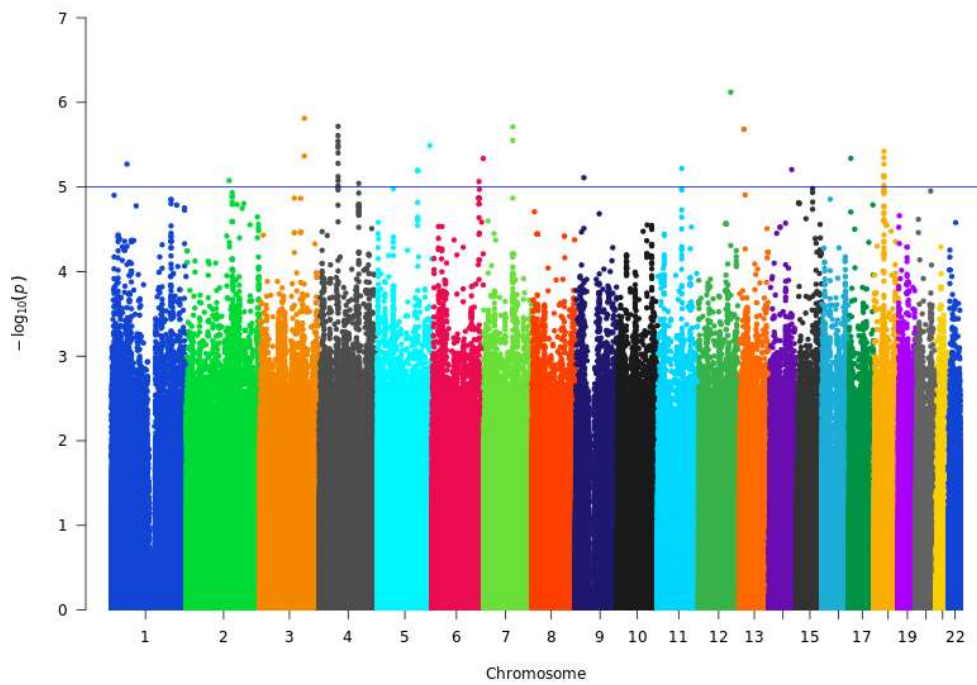


Figure S4. Manhattan plot of genome-wide association analysis for Skin aging index, related to Figure 7A.

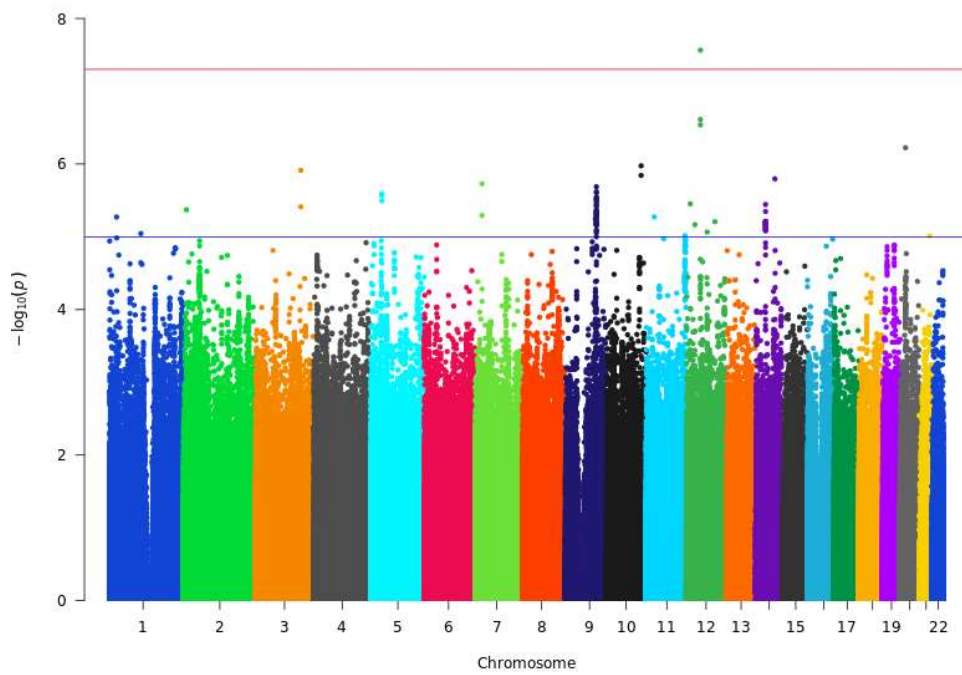


Figure S5. Manhattan plot of genome-wide association analysis for Hormone aging index, related to Figure 7A.

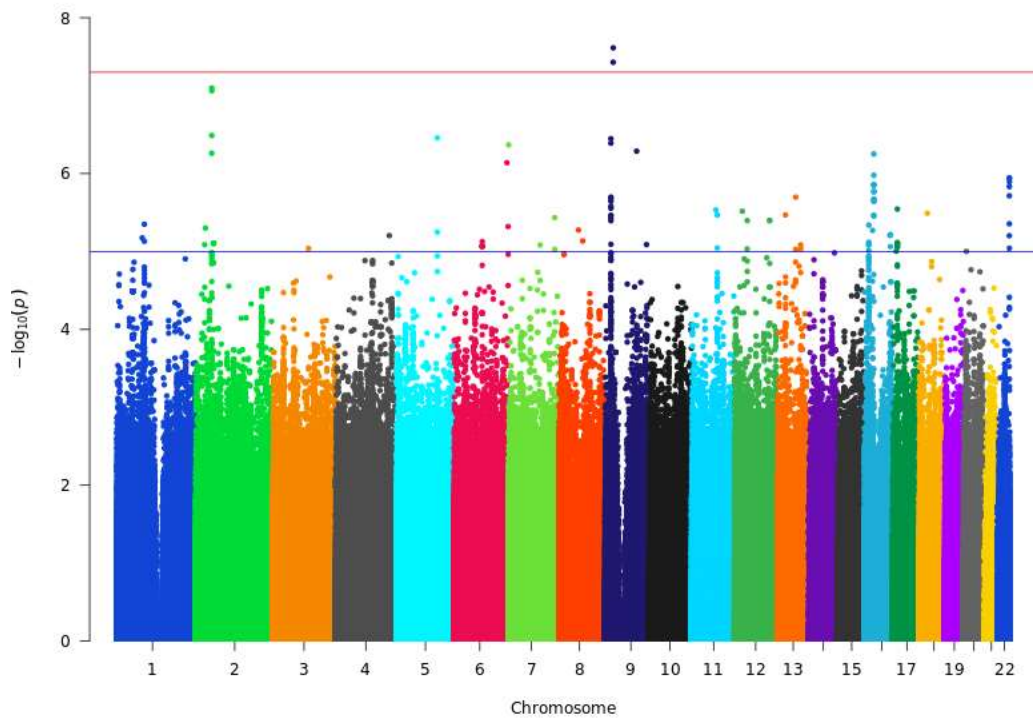


Figure S6. Manhattan plot of genome-wide association analysis for physical fitness aging index, related to Figure 7A.

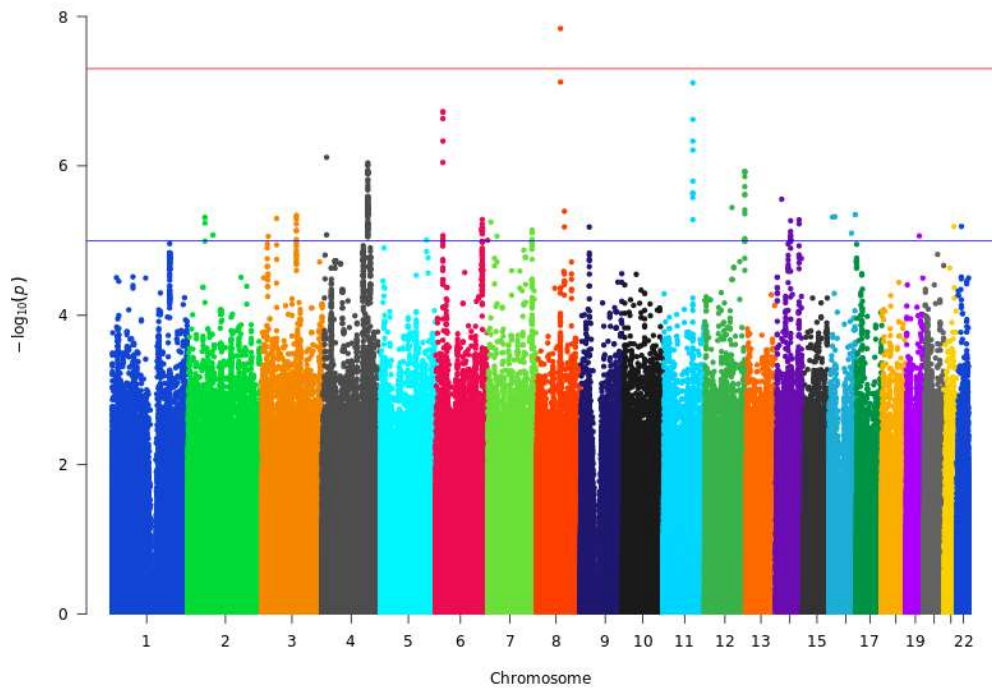


Figure S7. Manhattan plot of genome-wide association analysis for liver aging index, related to Figure 7A.

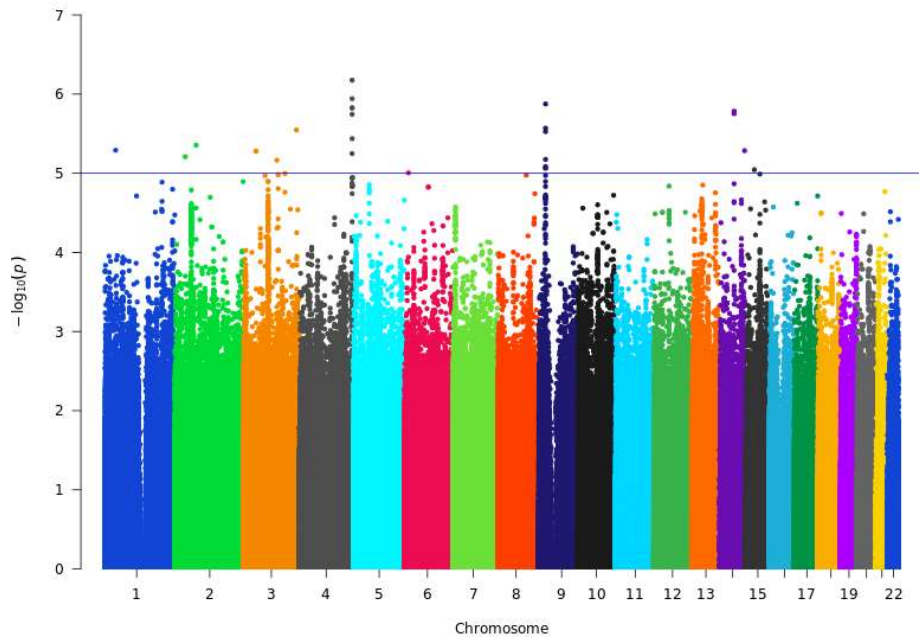


Figure S8. Manhattan plot of genome-wide association analysis for immune aging index, related to Figure 7A.

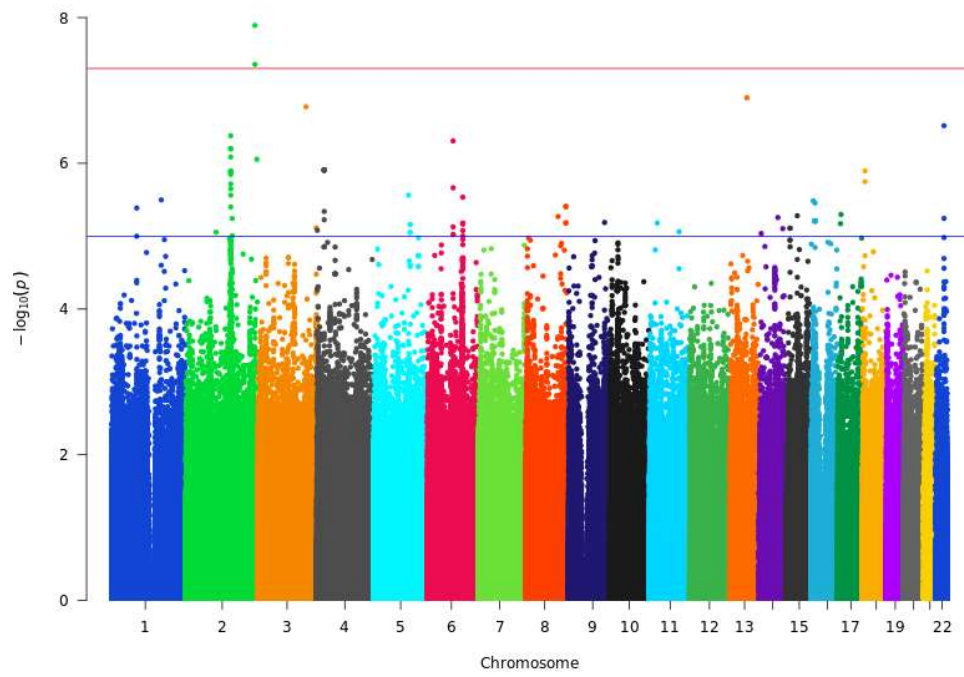


Figure S9. Manhattan plot of genome-wide association analysis for gut microbiome aging index, related to Figure 7A.

Table S1. Biomarkers from omics assessment, Related to Figure 1.

Data Type	Biomarker	No. of Biomarkers
Amino acid	Amino.1-Methylhistidine($\mu\text{mol/L}$)	39
	Amino.3-methylhistidine($\mu\text{mol/L}$)	
	Amino.Alanine($\mu\text{mol/L}$)	
	Amino.Arginine($\mu\text{mol/L}$)	
	Amino.Argininosuccinic_acid($\mu\text{mol/L}$)	
	Amino.Asparagine($\mu\text{mol/L}$)	
	Amino.Aspartic_acid($\mu\text{mol/L}$)	
	Amino.Carnosine($\mu\text{mol/L}$)	
	Amino.Citrulline($\mu\text{mol/L}$)	
	Amino.Cystathionine($\mu\text{mol/L}$)	
	Amino.Cystine($\mu\text{mol/L}$)	
	Amino.Ethanolamine($\mu\text{mol/L}$)	
	Amino.Glutamate($\mu\text{mol/L}$)	
	Amino.Glutamine($\mu\text{mol/L}$)	
	Amino.Glycine($\mu\text{mol/L}$)	
	Amino.Histidine($\mu\text{mol/L}$)	
	Amino.Homocysteine_level($\mu\text{mol/L}$)	
	Amino.Hydroxyproline($\mu\text{mol/L}$)	
	Amino.Isoleucine($\mu\text{mol/L}$)	
	Amino.Leucine($\mu\text{mol/L}$)	
	Amino.L-homocitrulline($\mu\text{mol/L}$)	
	Amino.Lysine($\mu\text{mol/L}$)	
	Amino.Methionine($\mu\text{mol/L}$)	
	Amino.Ornithine($\mu\text{mol/L}$)	
	Amino.Phenylalanine($\mu\text{mol/L}$)	
	Amino.Phosphoethanolamine($\mu\text{mol/L}$)	
	Amino.Phosphoserine($\mu\text{mol/L}$)	
	Amino.Proline($\mu\text{mol/L}$)	
	Amino.Sarcosine($\mu\text{mol/L}$)	
	Amino.Serine($\mu\text{mol/L}$)	
	Amino.Taurine($\mu\text{mol/L}$)	
	Amino.Threonine($\mu\text{mol/L}$)	
	Amino.Tryptophan($\mu\text{mol/L}$)	
Amino.Tyrosine($\mu\text{mol/L}$)		
Amino.valine($\mu\text{mol/L}$)		
Amino. α -aminoadipic_acid($\mu\text{mol/L}$)		
Amino. α -aminobutyric_Acid($\mu\text{mol/L}$)		
Amino. β -Alanine($\mu\text{mol/L}$)		
Amino. γ -Hydroxy_Lysine($\mu\text{mol/L}$)		
Vitamin	Vitamin.25-hydroxy_D(ng/mL)	10
	Vitamin.25-hydroxyD2(ng/mL)	
	Vitamin.25-hydroxyD3(ng/mL)	
	Vitamin.5-methyltetrahydrofolate(ng/mL)	
	Vitamin.A(ng/mL)	
	Vitamin.B1(ng/mL)	
	Vitamin.B2(ng/mL)	
	Vitamin.B5(ng/mL)	
	Vitamin.E(ng/mL)	
	Vitamin.Pyridoxine(ng/mL)	
	Hormone.12-Deoxycorticosterone_Test_Value(ng/mL)	
	Hormone.12-Deoxycortisol_test(ng/mL)	
	Hormone.18-hydroxyprogesterone_test_value(ng/mL)	
	Hormone.Androstenedione_test_value(ng/mL)	
	Hormone.Corticosterone_test_value(ng/mL)	
	Hormone.Progesterone(ng/mL)	

Hormone	Hormone.Serum_aldosterone_test_value(ng/mL)	13
	Hormone.Serum_cortisone_test_value(ng/mL)	
	Hormone.Serum_dehydroepiandrosterone(ng/mL)	
	Hormone.Serum_estradiol_test_value(ng/mL)	
	Hormone.Serum_estrone_test_value(ng/mL)	
	Hormone.Serum_hydrocortisone_test_value(ng/mL)	
	Hormone.Serum_testosterone_test_value(ng/mL)	
Microelement	Microelement.Arsenic(µg/L)	12
	Microelement.Cadmium(µg/L)	
	Microelement.Chromium(µg/L)	
	Microelement.Copper(mg/L)	
	Microelement.Iron(mg/L)	
	Microelement.Lead(µg/L)	
	Microelement.Magnesium(mg/l)	
	Microelement.Manganese(µg/L)	
	Microelement.Mercury(µg/L)	
	Microelement.Selenium(µg/L)	
	Microelement.Strontium(µg/L)	
	Microelement.Zinc(mg/l)	
	ECG	
ECG.Heart_rate(times/min)		
ECG.P-R_interval		
ECG.QRS_width(ms)		
ECG.QT_interval(ms)		
ECG.QTc_interval(ms)		
ECG.RV5+SV2_amplitude(mv)		
ECG.RV6_range(mv)		
ECG.SV2_range(mv)		
ECG.Systolic_pressure(mmHg)		
Clinical tests	Health.Albumin_concentration(g/L)	34
	Health.Alkaline_Phosphatase(U/L)	
	Health.Average_platelet_volume(fL)	
	Health.Basophil_absolute_counts(G/L)	
	Health.Basophil_percentage(%)	
	Health.Blood_urea_nitrogen_BUN(mmol/L)	
	Health.Direct_bilirubin(µmol/L)	
	Health.Eosinophil_absolute_counts(G/L)	
	Health.Fasting_blood_glucose(mmol/L)	
	Health.Globulin_concentration(g/L)	
	Health.High-density_lipoprotein(mmol/L)	
	Health.Indirect_bilirubin(µmol/L)	
	Health.Low-density_lipoprotein(mmol/L)	
	Health.Monocyte_counts(G/L)	
	Health.Monocyte_percentage(%)	
	Health.Neutrophil_percentage(%)	
	Health.Percentage_of_eosinophils(%)	
	Health.Percentage_of_lymphocytes(%)	
	Health.Platelet_count(G/L)	
	Health.Platelet_distribution_width(fL)	
	Health.Platelet_volume_ratio(%)	
	Health.Serum_alanine_aminotransferase(U/L)	
	Health.Serum_aspartate_aminotransferase(U/L)	
	Health.Serum_creatinine(µmol/L)	
	Health.Serum_total_bilirubin(µmol/L)	
	Health.Serum_uric_acid(µmol/L)	
	Health.The_total_number_of_neutrophils(G/L)	
Health.Total_cholesterol(mmol/L)		
Health.Total_number_of_lymphocytes(G/L)		

	Health.Triglyceride(mmol/L)	
	Health.Urine_pH	
	Health.USG	
	Health.White_blood_cell_count(G/L)	
	Health.γ-glutamyl_transpeptidase(U/L)	
Immune Repertoire measures	Immune.Summary_of_immune_cell_types	36
	Immune.Summary_of_immune_cells_diversity	
	Immune.Summary_of_immune_cells_homogeneity	
	Immune.Summary_of_VJ_genes_usage_diversity	
	Immune.uniq.Acute myeloid leukaemia	
	Immune.uniq.Allergy	
	Immune.uniq.Allergy_class	
	Immune.uniq.Aseptic meningitis	
	Immune.uniq.Autoimmune	
	Immune.uniq.Breast Cancer	
	Immune.uniq.Cancer	
	Immune.uniq.Celiac disease	
	Immune.uniq.Cytomegalovirus (CMV)	
	Immune.uniq.DENV1	
	Immune.uniq.DENV2	
	Immune.uniq.DENV3/4	
	Immune.uniq.Encounter for immunization	
	Immune.uniq.Epstein-Barr virus	
	Immune.uniq.Hepatitis C virus(HCV)	
	Immune.uniq.HTLV-I-Associated Myelopathy/Tropical Spastic Parap	
	Immune.uniq.Human immunodeficiency virus (HIV)	
	Immune.uniq.Inflammatory cranial neuropathy	
	Immune.uniq.Influenza	
	Immune.uniq.Lung cancer	
	Immune.uniq.M. tuberculosis	
	Immune.uniq.Melanoma	
	Immune.uniq.Multiple sclerosis (MS)	
	Immune.uniq.Neurosarcoidosis	
	Immune.uniq.Other	
	Immune.uniq.Pathogens	
	Immune.uniq.Polyradiculitis	
	Immune.uniq.Systemic lupus erythematosus(SLE)	
	Immune.uniq.Transverse myelitis	
Immune.uniq.Tuberculosis		
Immune.uniq.VZV meningoencephalitis		
Immune.uniq.Yellow fever virus		
Physical fitness	Inbody.Basal_metabolic_rate(kcal/d)	23
	Inbody.Body_fat(kg)	
	Inbody.Body_fat_rate(%)	
	Inbody.Body_mass_index	
	Inbody.Bust(cm)	
	Inbody.Extracellular_water_ratio_analysis	
	Inbody.Fat-free_body_weight(kg)	
	Inbody.Hip_circumference(cm)	
	Inbody.Inorganic_salt(kg)	
	Inbody.Muscle_mass(kg)	
	Inbody.Protein(kg)	
	Inbody.Skeletal_muscle(kg)	
	Inbody.Total_body_water(L)	
	Inbody.Waist_circumference(cm)	
	Inbody.Waist-to-hip_ratio	
	Phy.Hand_Grip_Test(kg)	
	Phy.Reaction_time(s)	

Phy.Single-legged with eyes closed (s)
Phy.Sit-and-reach_Test(cm)
Phy.Sit-up/Push_up_Test
Phy.Step_index
Phy.Vertical_jump_Test
Phy.Vital_capacity(mL)
Meta.Acidaminococcus_intestini
Meta.Actinobacillus_unclassified
Meta.Actinomyces_graevenitzii
Meta.Adlercreutzia_equolifaciens
Meta.Akkermansia_muciniphila
Meta.Alistipes_finegoldii
Meta.Alistipes_indistinctus
Meta.Alistipes_onderdonkii
Meta.Alistipes_putredinis
Meta.Alistipes_senegalensis
Meta.Alistipes_shahii
Meta.Alistipes_sp_AP11
Meta.Alistipes_unclassified
Meta.Alloprevotella_unclassified
Meta.Anaerostipes_hadrus
Meta.Anaerotruncus_colihominis
Meta.Anaerotruncus_unclassified
Meta.Bacteroidales_bacterium_ph8
Meta.Bacteroides_caccae
Meta.Bacteroides_cellulosilyticus
Meta.Bacteroides_clarus
Meta.Bacteroides_coprocola
Meta.Bacteroides_coprophilus
Meta.Bacteroides_dorei
Meta.Bacteroides_eggerthii
Meta.Bacteroides_faecis
Meta.Bacteroides_finegoldii
Meta.Bacteroides_fragilis
Meta.Bacteroides_intestinalis
Meta.Bacteroides_massiliensis
Meta.Bacteroides_nordii
Meta.Bacteroides_oleiciplenus
Meta.Bacteroides_ovatus
Meta.Bacteroides_plebeius
Meta.Bacteroides_salyersiae
Meta.Bacteroides_sp_2_1_22
Meta.Bacteroides_sp_3_1_19
Meta.Bacteroides_stercoris
Meta.Bacteroides_thetaiotaomicron
Meta.Bacteroides_uniformis
Meta.Bacteroides_vulgatus
Meta.Bacteroides_xylanisolvens
Meta.Barnesiella_intestinihominis
Meta.Bifidobacterium_adolescentis
Meta.Bifidobacterium_animalis
Meta.Bifidobacterium_bifidum
Meta.Bifidobacterium_longum
Meta.Bifidobacterium_pseudocatenulatum
Meta.Bilophila_unclassified
Meta.Bilophila_wadsworthia
Meta.Burkholderiales_bacterium_1_1_47
Meta.Butyricimonas_synergistica

Meta.Butyrvibrio_unclassified
Meta.Campylobacter_hominis
Meta.Catenibacterium_mitsuokai
Meta.Cellulophaga_unclassified
Meta.Chlorobium_phaeobacteroides
Meta.Citrobacter_freundii
Meta.Citrobacter_unclassified
Meta.Clostridiaceae_bacterium_JC118
Meta.Clostridiales_bacterium_1_7_47FAA
Meta.Clostridium_asparagiforme
Meta.Clostridium_bartlettii
Meta.Clostridium_bolteae
Meta.Clostridium_citroniae
Meta.Clostridium_clostridioforme
Meta.Clostridium_hathewayi
Meta.Clostridium_leptum
Meta.Clostridium_nexile
Meta.Clostridium_perfringens
Meta.Clostridium_amosum
Meta.Clostridium_sp_L2_50
Meta.Clostridium_symbiosum
Meta.Collinsella_aerofaciens
Meta.Collinsella_intestinalis
Meta.Collinsella_tanakaei
Meta.Collinsella_unclassified
Meta.Comamonas_unclassified
Meta.Coprobacillus_unclassified
Meta.Coprobacter_fastidiosus
Meta.Coprococcus_catus
Meta.Coprococcus_comes
Meta.Coprococcus_eutactus
Meta.Coprococcus_sp_ART55_1
Meta.Deinococcus_unclassified
Meta.Desulfovibrio_desulfuricans
Meta.Desulfovibrio_piger
Meta.Dialister_invisus
Meta.Dialister_succinatiphilus
Meta.Dorea_formicigenerans
Meta.Dorea_longicatena
Meta.Dorea_unclassified
Meta.Eggerthella_lenta
Meta.Eggerthella_unclassified
Meta.Enterobacter_aerogenes
Meta.Enterobacter_cloacae
Meta.Erysipelotrichaceae_bacterium_2_2_44A
Meta.Erysipelotrichaceae_bacterium_6_1_45
Meta.Escherichia_coli
Meta.Escherichia_unclassified
Meta.Eubacterium_biforme
Meta.Eubacterium_dolichum
Meta.Eubacterium_eligens
Meta.Eubacterium_hallii
Meta.Eubacterium_ramulus
Meta.Eubacterium_rectale
Meta.Eubacterium_siraeum
Meta.Eubacterium_sp_3_1_31
Meta.Eubacterium_ventriosum
Meta.Faecalibacterium_prausnitzii

Meta.Flavonifractor_plautii
Meta.Fusobacterium_mortiferum
Meta.Fusobacterium_nucleatum
Meta.Fusobacterium_ulcerans
Meta.Fusobacterium_varium
Meta.Gemella_unclassified
Meta.Granulicatella_unclassified
Meta.Haemophilus_haemolyticus
Meta.Haemophilus_parainfluenzae
Meta.Haemophilus_sputorum
Meta.Holdemania_filiformis
Meta.Holdemania_unclassified
Meta.Klebsiella_oxytoca
Meta.Klebsiella_pneumoniae
Meta.Klebsiella_unclassified
Meta.Lachnospiraceae_bacterium_1_1_57FAA
Meta.Lachnospiraceae_bacterium_1_4_56FAA
Meta.Lachnospiraceae_bacterium_2_1_58FAA
Meta.Lachnospiraceae_bacterium_3_1_46FAA
Meta.Lachnospiraceae_bacterium_3_1_57FAA_CT1
Meta.Lachnospiraceae_bacterium_5_1_63FAA
Meta.Lachnospiraceae_bacterium_6_1_63FAA
Meta.Lachnospiraceae_bacterium_7_1_58FAA
Meta.Lachnospiraceae_bacterium_8_1_57FAA
Meta.Lachnospiraceae_bacterium_9_1_43BFAA
Meta.Lactococcus_garvieae
Meta.Lactococcus_lactis
Meta.Leuconostoc_lactis
Meta.Megamonas_funiformis
Meta.Megamonas_hypermegale
Meta.Megamonas_rupellensis
Meta.Megamonas_unclassified
Meta.Megasphaera_elsdenii
Meta.Megasphaera_micronuciformis
Meta.Megasphaera_unclassified
Meta.Methanobrevibacter_smithii
Meta.Mitsuokella_multacida
Meta.Mitsuokella_unclassified
Meta.Odoribacter_splanchnicus
Meta.Odoribacter_unclassified
Meta.Oscillibacter_unclassified
Meta.Oxalobacter_formigenes
Meta.Pantoea_unclassified
Meta.Parabacteroides_distasonis
Meta.Parabacteroides_goldsteinii
Meta.Parabacteroides_johnsonii
Meta.Parabacteroides_merdae
Meta.Parabacteroides_unclassified
Meta.Paraprevotella_clara
Meta.Paraprevotella_unclassified
Meta.Paraprevotella_xylaniphila
Meta.Parasutterella_excrementihominis
Meta.Pedobacter_unclassified
Meta.Peptostreptococcaceae_noname_unclassified
Meta.Peptostreptococcus_stomatis
Meta.Peptostreptococcus_unclassified
Meta.Phascolarctobacterium_succinatutens
Meta.Porphyrromonas_asaccharolytica

	Meta.Porphyrmonas_bennonis	
	Meta.Porphyrmonas_uenonis	
	Meta.Prevotella_bivia	
	Meta.Prevotella_buccalis	
	Meta.Prevotella_copri	
	Meta.Prevotella_disiens	
	Meta.Prevotella_stercorea	
	Meta.Prevotella_timonensis	
	Meta.Pseudoflavonifractor_capillosus	
	Meta.Pyramidobacter_piscolens	
	Meta.Raoultella_ornithinolytica	
	Meta.Roseburia_hominis	
	Meta.Roseburia_intestinalis	
	Meta.Roseburia_inulinivorans	
	Meta.Roseburia_unclassified	
	Meta.Rothia_mucilaginosa	
	Meta.Ruminococcaceae_bacterium_D16	
	Meta.Ruminococcus_albus	
	Meta.Ruminococcus_bromii	
	Meta.Ruminococcus_callidus	
	Meta.Ruminococcus_gnavus	
	Meta.Ruminococcus_lactaris	
	Meta.Ruminococcus_obelum	
	Meta.Ruminococcus_sp_5_1_39BFAA	
	Meta.Ruminococcus_torques	
	Meta.Shigella_sonnei	
	Meta.species_shannon	
	Meta.Streptococcus_australis	
	Meta.Streptococcus_infantis	
	Meta.Streptococcus_mitis_oralis_pneumoniae	
	Meta.Streptococcus_parasanguinis	
	Meta.Streptococcus_salivarius	
	Meta.Streptococcus_sanguinis	
	Meta.Streptococcus_thermophilus	
	Meta.Subdoligranulum_unclassified	
	Meta.Sutterella_wadsworthensis	
	Meta.Turicibacter_unclassified	
	Meta.Veillonella_atypica	
	Meta.Veillonella_dispar	
	Meta.Veillonella_parvula	
	Meta.Veillonella_unclassified	
	Meta.Weissella_confusa	
Skin imaging features	Skin.Number_of_brown_spots_on_frontal_face	16
	Skin.Number_of_brown_spots_on_side_face	
	Skin.Number_of_pores_on_frontal_face	
	Skin.Number_of_pores_on_side_face	
	Skin.Number_of_porphyrins_on_frontal_face	
	Skin.Number_of_porphyrins_on_side_face	
	Skin.Number_of_red_areas_on_frontal_face	
	Skin.Number_of_red_areas_on_side_face	
	Skin.Number_of_spots_on_frontal_face	
	Skin.Number_of_spots_on_side_face	
	Skin.Number_of_textures_on_frontal_face	
	Skin.Number_of_textures_on_side_face	
	Skin.Number_of_UV_spots_on_frontal_face	
	Skin.Number_of_UV_spots_on_side_face	
	Skin.Number_of_wrinkles_on_frontal_face	
	Skin.Number_of_wrinkles_on_side_face	

Total number		403
--------------	--	-----

Table S2. Summary Statistics of Linear Model for biomarkers Contributed to Bas, Related to Figure 3.

Marker	k	q	s	r
ECG.Diastolic_pressure.mmHg._male	0.1616	67.1806	8.4432	0.1193
ECG.Diastolic_pressure.mmHg._female	0.0293	66.1470	7.9901	0.0174
ECG.Heart_rate.times.min._male	-0.0948	72.2018	10.2300	0.0606
ECG.Heart_rate.times.min._female	-0.1868	76.3215	9.6468	0.0898
ECG.P.R_interval_male	0.3465	144.2348	20.8028	0.1085
ECG.P.R_interval_female	0.2381	140.5487	18.5632	0.0596
ECG.QRS_width.ms._male	-0.1338	100.0389	9.2548	0.0944
ECG.QRS_width.ms._female	0.0478	82.6368	8.0438	0.0277
ECG.QT_interval.ms._male	0.4319	369.5136	23.8817	0.1177
ECG.QT_interval.ms._female	0.7579	363.6698	23.5485	0.1481
ECG.QTc_interval.ms._male	0.1799	402.8339	19.6679	0.0599
ECG.QTc_interval.ms._female	0.3090	407.5465	19.0186	0.0754
ECG.Systolic_pressure.mmHg._male	-0.0439	118.5647	10.6955	0.0257
ECG.Systolic_pressure.mmHg._female	0.0567	104.3424	9.9553	0.0270
Health.Fasting_blood_glucose.mmol.L._male	0.0248	4.5306	0.5996	0.2608
Health.Fasting_blood_glucose.mmol.L._female	0.0132	4.7012	0.3608	0.1703
Health.High.density_lipoprotein.mmol.L._male	-0.0032	1.3864	0.2523	0.0822
Health.High.density_lipoprotein.mmol.L._female	-0.0010	1.5933	0.3184	0.0142
Health.Low.density_lipoprotein.mmol.L._male	0.0122	2.4633	0.6032	0.1306
Health.Low.density_lipoprotein.mmol.L._female	0.0098	2.2902	0.5825	0.0799
Health.Total_cholesterol.mmol.L._male	0.0149	4.4019	0.8707	0.1113
Health.Total_cholesterol.mmol.L._female	0.0127	4.3080	0.8742	0.0688
Health.Triglyceride.mmol.L._male	0.0224	0.7366	1.0564	0.1369
Health.Triglyceride.mmol.L._female	0.0134	0.5803	0.5487	0.1148
Phy.Step_index_male	-0.0480	53.9618	8.4858	0.0313
Phy.Step_index_female	0.1956	48.9794	7.9274	0.1084
Health.Monocyte_percentage..._male	-0.0098	5.3526	1.2414	0.0518
Health.Monocyte_percentage..._female	-0.0079	4.8556	1.1367	0.0330
Health.Platelet_distribution_width.fL._male	0.0098	12.5018	1.9650	0.0328
Health.Platelet_distribution_width.fL._female	0.0366	11.4949	1.9461	0.0893
Health.Platelet_volume_ratio..._male	-0.0005	0.2822	0.0477	0.0662
Health.Platelet_volume_ratio..._female	-0.0011	0.3217	0.0545	0.0958
Hormone.12.Deoxycortisol_test.ng.mL._male	-0.0050	0.4349	0.1877	0.1648
Hormone.12.Deoxycortisol_test.ng.mL._female	-0.0033	0.3091	0.1813	0.0948
Hormone.Serum_cortisone_test_value.ng.mL._mal	-0.1236	28.4246	5.5501	0.1378
Hormone.Serum_cortisone_test_value.ng.mL._fem	-0.2521	32.5025	6.5249	0.1976
Hormone.Serum_hydrocortisone_test_value.ng.mL	-1.1400	127.9161	39.1360	0.1791
Hormone.Serum_hydrocortisone_test_value.ng.mL	-1.2453	117.8861	42.0207	0.1528
Health.Serum_creatinine.µmol.L._male	-0.1006	80.7789	9.7023	0.0676
Health.Serum_creatinine.µmol.L._female	-0.0660	55.9820	7.5765	0.0413
Health.Serum_uric_acid.µmol.L._male	-0.5446	427.7436	78.9646	0.0450
Health.Serum_uric_acid.µmol.L._female	-0.9037	317.1093	58.9065	0.0725
Hormone.12.Deoxycorticosterone_Test_Value.ng.n	-0.0007	0.0529	0.0239	0.1841
Hormone.12.Deoxycorticosterone_Test_Value.ng.n	-0.0006	0.0537	0.0321	0.0905
Hormone.Corticosterone_test_value.ng.mL._male	-0.1646	11.1810	5.6065	0.1805
Hormone.Corticosterone_test_value.ng.mL._femal	-0.1450	9.0989	4.6019	0.1622
Amino.1.Methylhistidine.µmol.L._male	-0.0709	8.0702	5.4533	0.0809
Amino.1.Methylhistidine.µmol.L._female	-0.0465	4.9583	3.8072	0.0635
Amino.3.methylhistidine.µmol.L._male	-0.0173	5.0905	1.3294	0.0809
Amino.3.methylhistidine.µmol.L._female	-0.0078	3.4937	1.1133	0.0365
Amino.Arginine.µmol.L._male	-0.0996	70.1292	19.3357	0.0322
Amino.Arginine.µmol.L._female	-0.2404	67.4376	19.4210	0.0644
Amino.Argininosuccinic_acid.µmol.L._male	-0.0004	0.0473	0.0338	0.0705
Amino.Argininosuccinic_acid.µmol.L._female	-0.0005	0.0514	0.0362	0.0706

Amino.Citrulline.µmol.L._male	0.0066	28.0781	6.6628	0.0062
Amino.Citrulline.µmol.L._female	0.0148	24.2906	6.6447	0.0116
Amino.Cystine.µmol.L._male	0.2933	17.5753	12.4531	0.1456
Amino.Cystine.µmol.L._female	0.0876	20.4719	11.0196	0.0414
Amino.Ethanolamine.µmol.L._male	-0.0294	9.7296	1.7906	0.1019
Amino.Ethanolamine.µmol.L._female	-0.0190	8.0497	1.9911	0.0496
Amino.Glutamate.µmol.L._male	0.5081	46.9563	33.6697	0.0939
Amino.Glutamate.µmol.L._female	0.2039	37.4580	22.6071	0.0470
Amino.Glycine.µmol.L._male	-0.6066	245.4963	54.4193	0.0695
Amino.Glycine.µmol.L._female	0.3465	223.9841	75.1498	0.0240
Amino.Isoleucine.µmol.L._male	-0.0262	74.5270	11.2221	0.0146
Amino.Isoleucine.µmol.L._female	-0.1522	62.9687	9.7029	0.0815
Amino.L.homocitrulline.µmol.L._male	-0.0011	0.1778	0.1307	0.0507
Amino.L.homocitrulline.µmol.L._female	-0.0014	0.1760	0.1286	0.0562
Amino.Lysine.µmol.L._male	0.1077	182.8136	32.9596	0.0204
Amino.Lysine.µmol.L._female	-0.1086	168.4146	32.5764	0.0174
Amino.Methionine.µmol.L._male	-0.0568	31.0201	5.1621	0.0686
Amino.Methionine.µmol.L._female	-0.0834	26.8077	4.7328	0.0915
Amino.Phenylalanine.µmol.L._male	-0.0107	59.7307	10.2883	0.0065
Amino.Phenylalanine.µmol.L._female	-0.1024	55.8616	9.0030	0.0592
Amino.Phosphoethanolamine.µmol.L._male	-0.0359	5.8741	2.8072	0.0796
Amino.Phosphoethanolamine.µmol.L._female	-0.0318	5.3041	1.6887	0.0977
Amino.Phosphoserine.µmol.L._male	-0.0017	0.4940	0.8550	0.0124
Amino.Phosphoserine.µmol.L._female	-0.0086	0.8402	1.1380	0.0395
Amino.Sarcosine.µmol.L._male	-0.0118	1.7558	0.9193	0.0798
Amino.Sarcosine.µmol.L._female	-0.0075	1.2881	0.7144	0.0550
Amino.Serine.µmol.L._male	-0.4299	129.2414	25.0996	0.1064
Amino.Serine.µmol.L._female	-0.5632	139.1127	28.2159	0.1035
Amino.Taurine.µmol.L._male	-0.2491	78.3802	24.6590	0.0630
Amino.Taurine.µmol.L._female	-0.2982	76.2959	18.1977	0.0852
Amino.Threonine.µmol.L._male	-0.3301	146.5094	31.8923	0.0645
Amino.Threonine.µmol.L._female	-0.4722	144.4463	37.3183	0.0659
Amino.Tryptophan.µmol.L._male	-0.1417	62.6431	9.8344	0.0896
Amino.Tryptophan.µmol.L._female	-0.2528	58.3670	9.1478	0.1427
Amino.Tyrosine.µmol.L._male	-0.0179	65.4340	12.2849	0.0091
Amino.Tyrosine.µmol.L._female	-0.1599	62.5485	11.3076	0.0735
Amino.α.aminoadipic_acid.µmol.L._male	0.0051	0.8035	0.4112	0.0773
Amino.α.aminoadipic_acid.µmol.L._female	0.0016	0.5892	0.2199	0.0382
Amino.α.aminobutyric_Acid.µmol.L._male	0.0724	20.0856	6.9013	0.0654
Amino.α.aminobutyric_Acid.µmol.L._female	0.0583	18.3700	6.8693	0.0442
Amino.β.Alanine.µmol.L._male	-0.0480	6.9572	2.1503	0.1380
Amino.β.Alanine.µmol.L._female	-0.0356	5.1696	1.6967	0.1089
Health.Albumin_concentration.g.L._male	-0.0867	50.6905	2.2758	0.2415
Health.Albumin_concentration.g.L._female	-0.0780	48.6265	2.6274	0.1393
Health.Indirect_bilirubin.µmol.L._male	-0.0343	14.9290	5.6481	0.0396
Health.Indirect_bilirubin.µmol.L._female	-0.0005	10.8584	4.1835	0.0006
Health.Serum_alanine_aminotransferase.U.L._male	-0.0031	27.4432	27.9248	0.0007
Health.Serum_alanine_aminotransferase.U.L._female	-0.0395	15.5127	11.6717	0.0160
Health.Serum_aspartate_aminotransferase.U.L._male	0.0240	24.4735	14.1783	0.0110
Health.Serum_aspartate_aminotransferase.U.L._female	-0.0512	21.5620	8.3764	0.0289
Health.γ.glutamyl_transpeptidase.U.L._male	0.5563	13.8225	29.5944	0.1219
Health.γ.glutamyl_transpeptidase.U.L._female	0.0151	16.0249	9.0304	0.0079
Microelement.Arsenic.µg.L._male	0.0496	0.4382	2.0536	0.1493
Microelement.Arsenic.µg.L._female	0.0229	1.0492	2.1231	0.0563
Microelement.Copper.mg.L._male	0.0017	0.7044	0.0852	0.1258
Microelement.Copper.mg.L._female	0.0020	0.7644	0.1194	0.0861
Microelement.Lead.µg.L._male	0.4821	7.3492	17.2852	0.1717
Microelement.Lead.µg.L._female	0.1265	13.6427	12.0085	0.0549

Microelement.Mercury.µg.L. _male	0.0713	-0.1457	1.8093	0.2392
Microelement.Mercury.µg.L. _female	0.0293	0.7704	1.2845	0.1181
Microelement.Selenium.µg.L. _male	0.6955	122.5525	24.8652	0.1722
Microelement.Selenium.µg.L. _female	0.2772	132.0436	25.9787	0.0556
Vitamin.25.hydroxy_D.ng.mL. _male	0.0810	19.1506	5.1321	0.0981
Vitamin.25.hydroxy_D.ng.mL. _female	0.1234	15.1325	5.3696	0.1190
Vitamin.25.hydroxyD2.ng.mL. _male	0.0103	0.2186	0.5534	0.1153
Vitamin.25.hydroxyD2.ng.mL. _female	0.0152	0.1315	0.6068	0.1297
Vitamin.5.methyltetrahydrofolate.ng.mL. _male	0.3463	5.7426	10.1357	0.2087
Vitamin.5.methyltetrahydrofolate.ng.mL. _female	0.5152	9.4413	16.5408	0.1604
Vitamin.A.ng.mL. _male	3.0658	529.1657	137.0569	0.1384
Vitamin.A.ng.mL. _female	2.7073	420.0754	113.3847	0.1236
Vitamin.B1.ng.mL. _male	0.1497	1.5633	7.1923	0.1290
Vitamin.B1.ng.mL. _female	0.1688	1.5128	8.0241	0.1091
Vitamin.B5.ng.mL. _male	0.5678	25.2515	13.7132	0.2504
Vitamin.B5.ng.mL. _female	0.3242	28.7601	12.9376	0.1296
Vitamin.E.ng.mL. _male	0.1160	7.1117	3.0026	0.2346
Vitamin.E.ng.mL. _female	0.1252	6.7182	2.8308	0.2248
Vitamin.Pyridoxine.ng.mL. _male	0.0471	2.3640	3.8560	0.0762
Vitamin.Pyridoxine.ng.mL. _female	0.0801	1.4070	7.1206	0.0586
Skin.Number_of_brown_spots_on_frontal_face_ma	0.3661	-0.7530	10.9577	0.2064
Skin.Number_of_brown_spots_on_frontal_face_fer	0.3514	-1.2182	10.7732	0.1530
Skin.Number_of_brown_spots_on_side_face_male	1.3462	65.6017	34.2968	0.2405
Skin.Number_of_brown_spots_on_side_face_fema	0.9004	45.9149	27.7358	0.1523
Skin.Number_of_pores_on_frontal_face_male	28.3984	527.7737	451.4112	0.3691
Skin.Number_of_pores_on_frontal_face_female	26.9280	189.6560	399.6327	0.3046
Skin.Number_of_pores_on_side_face_male	63.2276	223.1572	769.8496	0.4602
Skin.Number_of_pores_on_side_face_female	37.1508	-189.0976	450.9987	0.3641
Skin.Number_of_porphyrins_on_frontal_face_male	6.6437	-24.0033	70.9063	0.5091
Skin.Number_of_porphyrins_on_frontal_face_fema	5.8235	-19.8011	70.5565	0.3647
Skin.Number_of_porphyrins_on_side_face_male	6.5321	-16.1083	67.9684	0.5187
Skin.Number_of_porphyrins_on_side_face_female	5.2846	-36.1694	54.1455	0.4203
Skin.Number_of_red_areas_on_frontal_face_male	4.9529	-26.0132	82.5996	0.3540
Skin.Number_of_red_areas_on_frontal_face_female	1.1352	112.7441	94.5982	0.0569
Skin.Number_of_red_areas_on_side_face_male	3.8394	51.7069	72.8668	0.3156
Skin.Number_of_red_areas_on_side_face_female	0.8012	112.5605	54.5440	0.0695
Skin.Number_of_spots_on_frontal_face_male	2.7978	89.2776	41.5410	0.3912
Skin.Number_of_spots_on_frontal_face_female	2.5448	56.9430	42.6139	0.2727
Skin.Number_of_spots_on_side_face_male	2.6759	71.2106	37.8144	0.4078
Skin.Number_of_spots_on_side_face_female	2.2637	24.6901	29.5942	0.3412
Skin.Number_of_textures_on_frontal_face_male	-0.5568	3584.3553	1682.3635	0.0021
Skin.Number_of_textures_on_frontal_face_female	#####	3198.8521	1750.3963	0.0754
Skin.Number_of_textures_on_side_face_male	10.5034	2041.4564	1079.6030	0.0613
Skin.Number_of_textures_on_side_face_female	-6.2974	1299.3979	750.8974	0.0398
Skin.Number_of_UV_spots_on_frontal_face_male	4.4494	265.2726	88.5751	0.3022
Skin.Number_of_UV_spots_on_frontal_face_female	4.8553	259.1251	84.3683	0.2635
Skin.Number_of_UV_spots_on_side_face_male	3.8947	205.0202	66.4204	0.3471
Skin.Number_of_UV_spots_on_side_face_female	3.7803	155.1163	52.2119	0.3250
Skin.Number_of_wrinkles_on_frontal_face_male	8.2780	447.1068	261.2467	0.1961
Skin.Number_of_wrinkles_on_frontal_face_female	0.5430	490.1103	273.4794	0.0094
Skin.Number_of_wrinkles_on_side_face_male	13.4120	474.8446	338.8148	0.2424
Skin.Number_of_wrinkles_on_side_face_female	1.4934	499.4728	302.0173	0.0235
Inbody.Basal_metabolic_rate.kcal.d. _male	1.4140	1471.1202	180.2170	0.0488
Inbody.Basal_metabolic_rate.kcal.d. _female	2.7284	1098.0336	89.2916	0.1437
Inbody.Body_fat_rate... _male	0.2520	13.2941	6.0744	0.2503
Inbody.Body_fat_rate... _female	0.1577	23.4840	5.7972	0.1282
Inbody.Inorganic_salt.kg. _male	0.0043	3.4564	0.4541	0.0587
Inbody.Inorganic_salt.kg. _female	0.0114	2.3579	0.4059	0.1322

Inbody.Protein.kg. _male	0.0144	10.0751	1.1717	0.0765
Inbody.Protein.kg. _female	0.0128	7.0333	1.6794	0.0363
Inbody.Total_body_water.L. _male	0.0537	37.3098	4.6293	0.0757
Inbody.Total_body_water.L. _female	0.0991	24.5330	3.0419	0.1523
Phy.Reaction_time.s. _male	0.0024	0.4319	0.1072	0.1253
Phy.Reaction_time.s. _female	-0.0005	0.5502	0.0754	0.0288
Phy.Sit.up.Push_up_Test_male	-0.2229	30.6345	9.8967	0.0897
Phy.Sit.up.Push_up_Test_female	-0.5697	41.7382	8.5190	0.2833
Phy.Vertical_jump_Test_male	-1.1467	72.6712	10.1274	0.5310
Phy.Vertical_jump_Test_female	-0.3324	34.3628	7.6378	0.1888
Phy.Vital_capacity.mL. _male	#####	4363.5454	716.9549	0.1180
Phy.Vital_capacity.mL. _female	1.9555	2608.4134	484.6325	0.0178
Meta.Actinobacillus_unclassified_male	0.0000	0.0043	0.0277	0.0046
Meta.Actinobacillus_unclassified_female	-0.0003	0.0118	0.0306	0.0501
Meta.Alistipes_shahii_male	0.0012	0.4965	0.8111	0.0090
Meta.Alistipes_shahii_female	0.0106	0.4763	1.0314	0.0553
Meta.Bacteroides_eggerthii_male	0.0035	0.6567	3.2321	0.0068
Meta.Bacteroides_eggerthii_female	0.1412	-2.9628	4.1248	0.1810
Meta.Bacteroides_salysariae_male	0.0085	0.0729	0.7562	0.0715
Meta.Bacteroides_salysariae_female	0.0125	-0.0424	0.7526	0.0890
Meta.Bacteroides_sp_3_1_19_male	0.0052	0.0788	0.8829	0.0372
Meta.Bacteroides_sp_3_1_19_female	0.0145	-0.1967	0.8982	0.0863
Meta.Bacteroides_uniformis_male	0.0440	1.0554	4.2921	0.0650
Meta.Bacteroides_uniformis_female	0.1344	-0.3395	5.6530	0.1268
Meta.Clostridium_citroniae_male	0.0002	0.0056	0.0257	0.0420
Meta.Clostridium_citroniae_female	0.0003	0.0088	0.0522	0.0277
Meta.Clostridium_leptum_male	0.0060	-0.1167	0.6981	0.0548
Meta.Clostridium_leptum_female	-0.0047	0.2087	0.3622	0.0693
Meta.Clostridium_nexile_male	-0.0013	0.1347	0.2657	0.0321
Meta.Clostridium_nexile_female	0.0020	0.0498	0.5871	0.0179
Meta.Comamonas_unclassified_male	0.0000	0.0013	0.0032	0.0432
Meta.Comamonas_unclassified_female	0.0000	0.0021	0.0037	0.0700
Meta.Coprobacillus_unclassified_male	0.0003	-0.0008	0.0379	0.0539
Meta.Coprobacillus_unclassified_female	0.0001	0.0139	0.0787	0.0061
Meta.Eubacterium_eligens_male	0.0012	1.1221	2.8053	0.0028
Meta.Eubacterium_eligens_female	0.0101	1.0319	2.2195	0.0245
Meta.Haemophilus_parainfluenzae_male	0.0006	0.4461	1.7397	0.0022
Meta.Haemophilus_parainfluenzae_female	-0.0181	0.9563	1.0119	0.0955
Meta.Haemophilus_sputorum_male	0.0000	0.0028	0.0143	0.0036
Meta.Haemophilus_sputorum_female	-0.0003	0.0114	0.0188	0.0793
Meta.Leuconostoc_lactis_male	-0.0001	0.0053	0.0317	0.0151
Meta.Leuconostoc_lactis_female	-0.0001	0.0052	0.0174	0.0361
Meta.Prevotella_copri_male	-0.0456	18.0647	25.6889	0.0113
Meta.Prevotella_copri_female	-0.3079	22.2936	22.5729	0.0731
Meta.Roseburia_unclassified_male	0.0003	0.0510	0.2189	0.0093
Meta.Roseburia_unclassified_female	0.0016	0.0779	0.4500	0.0196
Meta.Streptococcus_australis_male	-0.0001	0.0085	0.0126	0.0737
Meta.Streptococcus_australis_female	0.0002	-0.0001	0.0152	0.0545
Meta.Streptococcus_thermophilus_male	-0.0027	0.1261	0.3470	0.0491
Meta.Streptococcus_thermophilus_female	-0.0067	0.2951	0.7172	0.0504
Meta.Subdoligranulum_unclassified_male	0.0331	0.6901	3.0175	0.0695
Meta.Subdoligranulum_unclassified_female	0.0222	1.4213	3.3013	0.0361
Meta.Alistipes_onderdonkii_male	0.0166	-0.0998	1.2062	0.0872
Meta.Alistipes_onderdonkii_female	0.0161	0.1786	1.6299	0.0531
Meta.Bacteroides_coprocola_male	-0.0610	5.3717	8.2548	0.0469
Meta.Bacteroides_coprocola_female	-0.1266	7.1806	8.3366	0.0814
Meta.Bacteroides_nordii_male	0.0005	0.0130	0.0944	0.0315
Meta.Bacteroides_nordii_female	-0.0003	0.0550	0.1437	0.0094

Meta.Bacteroides_uniformis_male	0.0440	1.0554	4.2921	0.0650
Meta.Bacteroides_uniformis_female	0.1344	-0.3395	5.6530	0.1268
Meta.Bifidobacterium_animalis_male	0.0001	0.0040	0.1283	0.0027
Meta.Bifidobacterium_animalis_female	-0.0007	0.0272	0.0884	0.0410
Meta.Bifidobacterium_longum_male	-0.0029	0.1779	0.2990	0.0613
Meta.Bifidobacterium_longum_female	-0.0013	0.1749	0.6663	0.0104
Meta.Clostridium_asparagiforme_male	0.0001	0.0244	0.1445	0.0031
Meta.Clostridium_asparagiforme_female	-0.0004	0.0487	0.1196	0.0162
Meta.Clostridium_citroniae_male	0.0002	0.0056	0.0257	0.0420
Meta.Clostridium_citroniae_female	0.0003	0.0088	0.0522	0.0277
Meta.Clostridium_hathewayi_male	-0.0009	0.0600	0.2543	0.0221
Meta.Clostridium_hathewayi_female	0.0059	-0.1127	0.4803	0.0656
Meta.Collinsella_aerofaciens_male	-0.0016	0.1117	0.1742	0.0588
Meta.Collinsella_aerofaciens_female	-0.0009	0.0854	0.1327	0.0356
Meta.Dorea_longicatena_male	-0.0006	0.0893	0.1622	0.0219
Meta.Dorea_longicatena_female	-0.0020	0.1373	0.2180	0.0483
Meta.Enterobacter_aerogenes_male	0.0001	0.0098	0.0745	0.0061
Meta.Enterobacter_aerogenes_female	0.0006	0.0053	0.2619	0.0118
Meta.Gemella_unclassified_male	0.0000	0.0005	0.0015	0.0401
Meta.Gemella_unclassified_female	0.0000	0.0007	0.0022	0.0410
Meta.Holdemania_filiformis_male	0.0003	0.0219	0.0613	0.0358
Meta.Holdemania_filiformis_female	0.0004	0.0236	0.0857	0.0252
Meta.Klebsiella_pneumoniae_male	-0.0065	0.8595	2.3513	0.0176
Meta.Klebsiella_pneumoniae_female	0.0001	0.5765	2.4402	0.0003
Meta.Lachnospiraceae_bacterium_3_1_46FAA_male	0.0008	0.0093	0.1548	0.0337
Meta.Lachnospiraceae_bacterium_3_1_46FAA_female	0.0012	0.0103	0.1648	0.0397
Meta.Megamonas_unclassified_male	-0.0078	1.3009	3.1914	0.0154
Meta.Megamonas_unclassified_female	-0.0210	1.2383	2.0241	0.0557
Meta.Mitsuokella_multacida_male	0.0009	-0.0093	0.1389	0.0413
Meta.Mitsuokella_multacida_female	-0.0002	0.0220	0.1550	0.0063
Meta.Odoribacter_splanchnicus_male	-0.0005	0.7519	0.9576	0.0034
Meta.Odoribacter_splanchnicus_female	-0.0105	1.2947	1.1164	0.0504
Meta.Pantoea_unclassified_male	0.0000	0.0040	0.0146	0.0059
Meta.Pantoea_unclassified_female	0.0000	0.0027	0.0108	0.0036
Meta.Parabacteroides_merdae_male	-0.0053	1.3754	1.6817	0.0199
Meta.Parabacteroides_merdae_female	0.0161	0.9664	1.7873	0.0485
Meta.Ruminococcus_obeum_male	-0.0010	0.1235	0.1323	0.0463
Meta.Ruminococcus_obeum_female	-0.0006	0.1228	0.1395	0.0238
Meta.Ruminococcus_sp_5_1_39BFAA_male	-0.0032	0.2331	0.4032	0.0506
Meta.Ruminococcus_sp_5_1_39BFAA_female	0.0007	0.0884	0.4033	0.0094
Meta.Streptococcus_australis_male	-0.0001	0.0085	0.0126	0.0737
Meta.Streptococcus_australis_female	0.0002	-0.0001	0.0152	0.0545
Meta.Streptococcus_salivarius_male	0.0012	0.0905	0.3370	0.0235
Meta.Streptococcus_salivarius_female	-0.0009	0.1302	0.2360	0.0200
Meta.Streptococcus_thermophilus_male	-0.0027	0.1261	0.3470	0.0491
Meta.Streptococcus_thermophilus_female	-0.0067	0.2951	0.7172	0.0504
Meta.Subdoligranulum_unclassified_male	0.0331	0.6901	3.0175	0.0695
Meta.Subdoligranulum_unclassified_female	0.0222	1.4213	3.3013	0.0361
Meta.Weissella_confusa_male	-0.0001	0.0064	0.0233	0.0388
Meta.Weissella_confusa_female	0.0000	0.0001	0.0103	0.0226

Table S3. list of features in the National Health and Nutrition Examination Survey (NHANES) data used for biological age constructions, Related to Figure 6.

Organ/system	Cardiovascular system	Kidney	Liver
Features	Triglyceride	Health.Serum_creatinine(umol/L)	Health.γ-glutamyl_transpeptidase(U/L)
	Low.density_lipoprotein	Health.Serum_uric_acid(umol/L)	Health.Serum_aspartate_aminotransferase(U/L)
	Fasting_blood_glucose		Health.Serum_alanine_aminotransferase(U/L)
	High.density_lipoprotein		Health.Albumin_concentration(g/L)
	Systolic_pressure		
	Diastolic_pressure		
	Total_cholesterol		

Table S4. Summary statistics of pathway based association for organ/system's biological ages, Related to Figure 7B.

Organ/system	Set	No.SNPs	Chisq(Obs)	Pvalue	opSNP.Pvalu	TopSNP
Cardiovascular_Age	KEGG MATURITY ONSET DIABETES OF THE YOUNG	30	70.0483	0.017941	0.009192	rs11983558
	KEGG BASAL_CELL_CARCINOMA	45	90.6065	0.025851	5.46E-06	rs138802825
	KEGG TGF BETA SIGNALING PATHWAY	59	112.592	0.035451	0.001292	rs57581393
	KEGG BLADDER CANCER	31	60.2848	0.043008	0.007379	rs72841224
Nutrition_Metabolic_Age	KEGG CYSTEINE AND METHIONINE METABOLISM	25	48.3048	0.0318	0.01219	rs13218908
	KEGG STARCH AND SUCROSE METABOLISM	50	86.5926	0.028652	0.002585	rs365475
	KEGG GLYCEROLIPID METABOLISM	65	110.792	0.023567	0.008383	rs150572222
	KEGG BUTANOATE METABOLISM	84	166.012	0.021306	0.0009824	rs7970937
	KEGG ABC TRANSPORTERS	75	152.045	0.032159	0.001976	rs4147922
	KEGG CELL CYCLE	43	95.0633	0.02306	0.001993	rs74116832
	KEGG OOCYTE MEIOSIS	43	95.0633	0.02306	0.001993	rs74116832
	KEGG UBIQUITIN MEDIATED PROTEOLYSIS	43	95.0633	0.02306	0.001993	rs74116832
	KEGG PROGESTERONE MEDIATED OOCYTE MATURATION	43	95.0633	0.02306	0.001993	rs74116832
	KEGG MATURITY ONSET DIABETES OF THE YOUNG	30	60.2343	0.0393	0.001455	rs10949621
Renal_Age	KEGG PHENYLALANINE METABOLISM	83	174.455	0.014044	0.000294	rs4646672
	KEGG GLYCEROPHOSPHOLIPID METABOLISM	95	162.069	0.039153	0.001402	rs4479310
	KEGG OTHER GLYCAN DEGRADATION	46	94.0961	0.039539	0.001857	rs74001528
	KEGG ARGININE AND PROLINE METABOLISM	24	49.9878	0.044624	0.007931	rs10864489
	KEGG GLUTATHIONE METABOLISM	24	49.9878	0.044624	0.007931	rs10864489
Skin_age	KEGG GLYCOSAMINOGLYCAN DEGRADATION	159	276.621	0.020481	0.00248	rs12949669
	KEGG HOMOLOGOUS RECOMBINATION	26	57.3072	0.017327	0.001586	rs12044708
	KEGG TASTE TRANSDUCTION	39	76.6306	0.044459	0.00801	rs11771952
Sex_Hormone_Age	KEGG SPHINGOLIPID METABOLISM	48	114.16	0.005045	0.0001854	rs2267158
	KEGG ONE CARBON POOL BY FOLATE	29	71.9906	0.019235	0.0002158	rs12053233
	KEGG TAURINE AND HYPOTAURINE METABOLISM	16	38.5143	0.0194	0.01514	rs116707649
	KEGG ALPHA LINOLENIC ACID METABOLISM	51	112.568	0.020987	0.0007703	rs2412639
	KEGG SYSTEMIC LUPUS ERYTHEMATOSUS	52	93.8675	0.038718	0.002547	rs16829984
	KEGG PYRIMIDINE METABOLISM	61	98.5754	0.045954	0.0002893	rs11191561
Physical_Fitness_Age	KEGG ETHER LIPID METABOLISM	82	134.79	0.049638	0.0009804	rs77456161
	KEGG SNARE INTERACTIONS IN VESICULAR TRANSPORT	19	55.5724	0.002098	8.22E-05	rs57099027
	KEGG ONE CARBON POOL BY FOLATE	29	102.481	0.00255	0.001125	rs3821321
	KEGG HOMOLOGOUS RECOMBINATION	26	58.5481	0.015294	0.004803	rs12044708
	KEGG GLYCOSAMINOGLYCAN DEGRADATION	159	250.217	0.043254	0.0009433	rs149829242
	KEGG NATURAL KILLER CELL MEDIATED CYTOTOXICITY	20	39.0931	0.047365	0.01126	rs34635139
	KEGG PRIMARY IMMUNODEFICIENCY	20	39.0931	0.047365	0.01126	rs34635139
Immune_Age	KEGG ALPHA LINOLENIC ACID METABOLISM	51	95.5669	0.047668	0.005651	rs2412639
	KEGG O GLYCAN BIOSYNTHESIS	16	30.8211	0.045526	0.0007286	rs150328373
	KEGG PYRIMIDINE METABOLISM	61	109.997	0.021738	0.003223	rs116993824
	KEGG TAURINE AND HYPOTAURINE METABOLISM	16	39.3486	0.017351	0.005818	rs66535774
Liver_Age	KEGG LYSOSOME	11	35.79	0.009789	0.006234	rs2863981
	KEGG CYSTEINE AND METHIONINE METABOLISM	25	44.7192	0.048691	0.01316	rs2298886
	KEGG OTHER GLYCAN DEGRADATION	46	92.8653	0.041716	0.003117	rs2015651
	KEGG FATTY ACID METABOLISM	97	174.493	0.038589	0.002369	rs72943224
	KEGG VASOPRESSIN REGULATED WATER REABSORPTION	235	392.012	0.019571	0.0009383	rs11645015
	KEGG VALINE LEUCINE AND ISOLEUCINE BIOSYNTHESIS	8	20.7413	0.018684	0.001918	rs139768419
Gut_Microbiome_Age	KEGG CIRCADIAN RHYTHM MAMMAL	248	432.625	0.016113	0.0005074	rs78829057
	KEGG PYRIMIDINE METABOLISM	61	119.309	0.011741	0.005289	rs10883831
	KEGG TAURINE AND HYPOTAURINE METABOLISM	16	36.659	0.02489	0.01346	rs2024635
	KEGG ETHER LIPID METABOLISM	82	139.257	0.040743	0.0001914	rs140114409
	KEGG INTESTINAL IMMUNE NETWORK FOR IGA PRODUCT	54	90.2721	0.045671	4.35E-05	rs2256024
	KEGG TYPE I DIABETES MELLITUS	54	90.2721	0.045671	4.35E-05	rs2256024
	KEGG ASTHMA	54	90.2721	0.045671	4.35E-05	rs2256024
	KEGG ALLOGRAFT REJECTION	54	90.2721	0.045671	4.35E-05	rs2256024
	KEGG GRAFT VERSUS HOST DISEASE	54	90.2721	0.045671	4.35E-05	rs2256024
	KEGG GLYCOLYSIS GLUCONEOGENESIS	20	35.6465	0.047472	0.00245	rs36000727
	KEGG PYRUVATE METABOLISM	20	35.6465	0.047472	0.00245	rs36000727
	KEGG PROPANOATE METABOLISM	20	35.6465	0.047472	0.00245	rs36000727
	KEGG O GLYCAN BIOSYNTHESIS	16	30.538	0.047631	0.0005347	rs112258230

Table S5. The sample sizes of each category, Related to Figure 2.

Organ/system ages	No. of biomarkers	Sample type	Measurement method	Sample size	No. of male	No. of female
liver age	47	blood	blood chemical test,	2,599	1,261	1,338
cardiovascular age	16	blood	EEG, blood chemical test	1,535	700	835
renal age	8	blood	blood chemical test, LC-MS	2,514	1,236	1,278
nutrition metablomic age	22	blood	LC-MS, blood routine test	4,055	1,952	2,103
immune age	55	blood	immune repertoire sequencing, blood routine and chemical test	2,265	1,105	1,160
sex hormone age	7	blood	LC-MS	4,059	1,955	2,104
gut microbiome age	210	stool	metagenome sequencing	2,121	1,024	1,097
skin age	16	facial skin	Visia skin analysis system	1,766	824	942
physical fitness age	22	/	phycal fitnessl tests and microbiobio body composition test	2,046	984	1,062
Total sample size				4,066	1,957(48%)	2,109(52%)